Statistical Methods for Film Grain Noise Removal and Generation

by

Jacky Chun Kit Yan

A thesis submitted in conformity with the requirements
for the degree of Master of Applied Science
Graduate Department of Electrical and Computer Engineering
University of Toronto

Statistical Methods for Film Grain Noise Removal and Generation
by Jacky Chun Kit Yan
Master of Applied Science, 1997
Department of Electrical and Computer Engineering, University of Toronto

Abstract

This thesis deals with noise filtering and generation for signal-dependent film grain noise that is present in photographic images. For noise filtering, two new filters are proposed. The first filter is based on minimizing a higher-order statistics (H.O.S.) based criterion that is an extension of the second-order statistics based criterion. Another filtering approach is to combine a new local-statistics based technique with the generalized homomorphic transformation. The filter mask is adaptive to signal activities and can be extended to handle color image. Simulation results show that these new filters perform better than existing ones. Finally, for noise generation, which has applications in television and motion picture productions, a new procedure is successfully applied in grayscale and color images to estimate noise parameter using H.O.S. It is found that these two images (corrupted photographic image and image with artificial noise added) have similar noise level and visual appearance.

Acknowledgment

I wish to express my sincere gratitude to my supervisor, Prof. D. Hatzinakos, for his insightful guidance, advice, and encouragement during the development of this thesis. I am also grateful to Prof. A. N. Venetsanopoulos, Prof. Pankaj, and Prof. Dawson, for reviewing my work and for offering their valuable comments and suggestions.

Special thanks also go to Erwin, Wing, Richard, Wilson, Henry, Davy, Vineet, and my old friend Anthony for their friendly support, and making my stay in the communications group an enjoyable one. I would also like to thank Dimitrios from the DSP lab for helping me to print the color images.

The financial support of the Natural Sciences and Engineering Research Council of Canada, and of Prof. Hatzinakos are also gratefully acknowledged.

Last, but not least, my warm thanks go to my family and Enid for their care and support.

Contents

List of Figures

List of Tables

Chapter 1

Introduction

1.1 Image Processing in Signal-Dependent Noise

The problem of extracting information from noisy signals has led to the development of many techniques, and most of which have been applied to image processing. Traditional techniques for processing of corrupted images have primarily assumed additive signal-independent noise. These are well developed and applied in applications such as detection, filtering, enhancement, and prediction.

In contrast to the signal-independent, additive noise model assumed in most image processing algorithms, many physical noise processes are inherently signal-dependent [1]. For example, film grain noise that is present in photographic images has been modeled as Gaussian, with a standard deviation proportional to the square root of the signal [10, 11, 12, 13]. There are basically two options in processing signals degraded by signal-dependent noise : (1) disregard the dependence of the noise on the signal and treat it as a signal-independent noise; or (2) develop specific techniques that take into account the dependence of noise on the signal. In the first case, it was shown in [14] that failure to include signal-dependence of the noise pays a price in performance. In the latter case, two approaches that have been used in

image processing are the derivation of optimum filters for signal-dependent noise, and the alternative approach of first transforming the signal-dependent noise model to an equivalent signal-independent noise model and then apply filtering algorithms designed for signal-independent noise.

A popular representation for signal-dependent film grain noise is to model the noise term as a product of a function of the original signal and a statistically independent noise process [10]. Modifications were made to standard techniques designed for additive signal-independent noise to take the signal-dependence of noise into account. Expressions for various optimal estimators [14] (MMSE estimator, MAP estimator, ML estimator), Wiener filter [10, 16], and matched filter [11] for images corrupted by signal-dependent film grain noise were derived. Because the resulting structures of the optimal estimators are more complicated than those for signal-independent noise, suboptimal estimators have been proposed. [17]

Another approach to remove signal-dependent film grain noise is to first perform a point-wise nonlinear transformation whose purpose is to make the transformed noise additive and signal-independent. This technique, called homomorphic image processing, was initially applied to decouple signals and multiplicative noise (as in speckle images). The corresponding transformation can be shown to be logarithmic. Generalized homomorphic transformation was developed to transform different forms of signal-dependent noise to approximately additive signal-independent noise [19, 20, 21]. When this is done, standard processing techniques for additive noise can take place, which is then followed by an inverse transformation to change the filtered image back to the original domain. [11, 12, 13]

1.2 Origin and Noise Model for Signal-Dependent Film Grain Noise

1.2.1 Origin of Film Grain Noise

Image detection and recording by film relies upon the properties of silver halides [2]. When the film is exposed to light, the silver halide grains absorb optical energy and undergo a complex physical change. The grains that have absorbed a sufficient amount of energy contain tiny patches of metallic silver called development centers. When the exposed film is developed, the existence of a single development center in a silver halide grain can precipitate the change of the entire grain to metallic silver. After development, the film is "fixed" by chemical removal of the remaining silver halide grains.

The recording property of photographic film depends on the optical density D of the developed silver halide grains or the dye clouds. However, there is an inherent randomness in the distribution of the silver grains. Due to the statistical character of the photographic process, the silver grains are randomly located in distance from one another in the film emulsion, and they behave randomly under conditions of exposure and development. This randomness is referred to as film grain noise.

The optical density D is defined as: [3]

$$D = \log_{10} \frac{I_1}{I_2} \tag{1.1}$$

where I_1 is the intensity of a reference source of light and I_2 is the intensity of light transmitted through or reflected from a film when illuminated by the reference source I_1. A high optical density implies a small value of I_2 and hence a high density of silver deposits. Because images are normally represented in the light intensity domain I:

$$I = \frac{I_2}{I_1} \tag{1.2}$$

and are within the range $[0, 1]$, optical density D and intensity I are related by:

$$D = -\log_{10} I \tag{1.3}$$

The visual sensation of nonuniformity in the developed photographic film is called graininess, and an objective measure of the noise is referred to as granularity [4]. To obtain granularity of a film requires the measurement of the density across an uniformly exposed and developed film. Due to the statistical nature of the noise, the measured image r is observed to distribute randomly about the mean density μ_r. If the noise is assumed Gaussian and zero mean, the probability density distribution of r is

$$p(r) = \frac{1}{\sqrt{2\pi\sigma_r^2}} exp\left[\frac{-(r-\mu_r)^2}{2\sigma_r^2}\right] \tag{1.4}$$

Regardless of the type of assumed statistics, the rms granularity, σ_r, defined as

$$\sigma_r = \sqrt{\frac{1}{N^2}\sum_{x=1}^{N}\sum_{y=1}^{N} r(x,y)^2 - \mu_r^2} \tag{1.5}$$

is often used to measure the film's granularity. The property of the noise is such that the rms granularity is not a constant and is shown to vary with the mean density.

1.2.2 Noise Model for Signal-Dependent Film Grain Noise

Since the formation of an image on photographic film is a highly complex optical and chemical process, modeling this process with a high degree of accuracy, if at all possible, often results in models that are too complex and unsuitable for use in any mathematical processing. On the other hand, the reliability of restoration techniques is directly related to the degree to which the underlying mathematical model simulates the actual physical process. Therefore, oversimplifying the model makes the restoration technique very suboptimal.

As outlined previously, formation of film grain noise is a very complicated process. More physically appropriate models that take into account the distribution of grain size [5], the crowding effects of real grains at high densities for monolayers and multilayers [6, 7], and the arbitrary geometry of film grains [8], do not appear to be mathematically attractive in image processing. However, there are a few observations which can be stated about film grain noise in practical situations: [3]

- Film grains are assumed to distribute randomly, that is without crowding or clumping. The distribution is Poissonian that in the limit is approximated by a Gaussian process (Central Limit Theorem) with mean μ_r and variance σ_r^2.
- The noise variance is not a constant but varies with the mean density μ_r.
- Film grain noise is a white noise process in the sense that density measurements in different spatial positions in photographic film are statistically uncorrelated provided the samples are spaced farther apart than the grain size of the film. This is usually the case for typical scanners as their resolution is not high enough to discriminate individual film grains (grain size $\approx 0.1 - 1\mu m$).

There are basically three noise models that have been reported to characterize the signal-dependence of film grain noise. A brief discussion is as follows.

Low-Contrast Noise Model

Falconer [16] employed a low-contrast image assumption in an attempt to find a mathematical representation for grain noise. Starting from the exposing intensity and using physical arguments, Falconer expressed the observed density D as a sum of three components:

$$D = \text{ bias } + \text{ signal } + \text{ noise} \tag{1.6}$$

where each quantity is related to the amount of exposure and physical properties of film.

Autoregression Noise Model

In this case the noise $n(x, y)$ is represented as a two-dimensional homogeneous random field that satisfies the difference equation: [9]

$$n(x+1,y)+n(x-1,y)+n(x,y+1)+n(x,y-1)-(4+K^2)n(x,y) = Cw(x,y) \tag{1.7}$$

where K, C are parameters and $w(x, y)$ is a zero mean white Gaussian noise. The above difference equation is then transformed to a two-dimensional autoregression model. To estimate paramters of K and C, which are assumed to vary with the signal, autocorrelation of film grain noise data obtained from experiments and that from the above theretical model are used.

Additive Signal-Modulated Noise Model

A frequently used mathematical model for signal-dependent noise is given by [10, 11, 12, 13]

$$r = s + kf(s)n \tag{1.8}$$

where r is the observed signal, s is the signal, $f(s)$ is a zero-memory function, n is a signal-independent Gaussian noise process, and k is a scalar constant:

$$k \propto \sqrt{a/A} \tag{1.9}$$

a/A is the ratio of the grain size to the scanning aperture. Fig. 1.1 shows the signal-dependent noise model. The random noise n is usually assumed to be Gaussian with zero mean and unit variance. Notice the noise n is amplitude-modulated by the product of k times the nonlinear function $f(s)$ of the ideal image s. For film grain noise, the nonlinear function $f(s)$ takes the form

$$f(s) = s^p \tag{1.10}$$

where p is usually between 0.2 and 0.7 [14, 15] to give the following film grain noise model:

$$r = s + ks^p n \tag{1.11}$$

For the so-called ideal film grain noise, $p = 0.5$, and the model becomes

$$r = s + k\sqrt{s}n \tag{1.12}$$

Because of the popularity of this model, and its ability to describe the magnitude dependence of noise on signal, this additive signal-modulated model is assumed throughout the thesis.

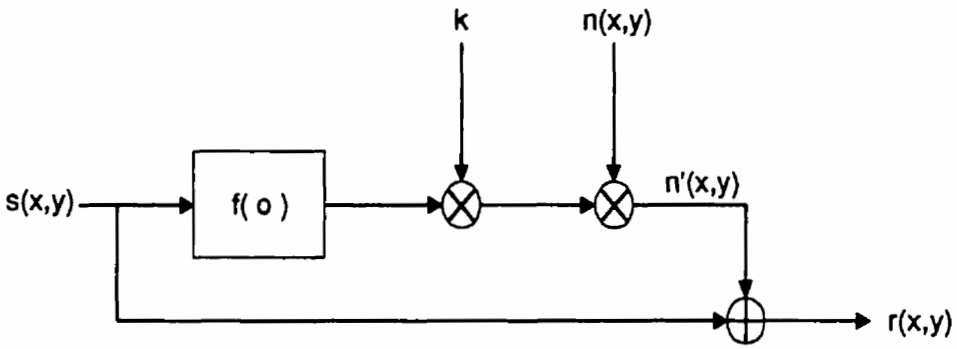

Figure 1.1: Noise model for signal-dependent film grain noise.

1.3 Existing Methods of Noise Filtering

Since film grain noise is inherently signal-dependent, noise suppression using standard techniques for signal-independent noise results in poor performance. Various techniques have been proposed, which can be classified into two approaches. The first approach is to modify conventional image restoration methods to take into account the dependence of noise on signal; The second approach is to first perform a pointwise transformation on the image such that the noise in the transformed image becomes additive signal-independent. Once the transformation is performed, conventional restoration techniques designed for additive noise can then be applied. These techniques are outlined below.

1.3.1 Noise Filtering in Density Domain

The following is a list of techniques that are modifications of those designed for additive signal-independent noise. Noise filtering is carried out in the density domain.

Wiener Filtering

Given an observed noisy version $r(x,y)$ of a noiseless ideal image $s(x,y)$, the objective of the Wiener filter is to produce an estimate $\hat{s}(x,y)$ which minimizes the mean of the squared error $[\hat{s}(x,y) - s(x,y)]^2$. The form of the ideal image or signal $s(x,y)$ is unknown, but its spectral density, and that of the noise are assumed known. The two-dimensional Wiener filter has a spatial frequency domain transfer function of the form

$$W(u,v) = \frac{\phi_{rs}(u,v)}{\phi_{rr}(u,v)} \tag{1.13}$$

The terms $\phi_{rs}(u,v)$ and $\phi_{rr}(u,v)$ represent the cross-spectral density of $r(x,y)$ with $s(x,y)$, and the spatial density of $r(x,y)$ respectively.

Walkup and Choens [10] assumed the noise model to be the additive signal-modulated noise model, repeated here for convenience:

$$r(x,y) = s(x,y) + kf[s(x,y)]n(x,y) \tag{1.14}$$

Since in this model the noise $n(x,y)$ is assumed zero mean and statistically independent of the ideal image, it can easily be shown that $\phi_{rs} = \phi_{ss}$. As a result, the two-dimensional Wiener filter has the following transfer function

$$W(u,v) = \frac{\phi_{ss}(u,v)}{\phi_{ss}(u,v) + k^2\phi_{s's'}(u,v) * \phi_{nn}(u,v)} \tag{1.15}$$

with $\phi_{s's'}$ represents the spectral density of $s'(x,y) = f[s(x,y)]$. Assuming further that the noise process $n(x,y)$ is white, that is $\phi_{nn}(u,v) = N_0$, then the transfer function may be simplified to

$$W(u,v) = \frac{\phi_{ss}(u,v)}{\phi_{ss}(u,v) + k^2\overline{(s')^2}N_0} \tag{1.16}$$

where $\overline{(s')^2}$ is the mean squared value of $s'(x,y)$.

Simulations have been performed on images degraded according to the additive signal-modulated noise model with the function

$$f(s) = s^{1/3} \tag{1.17}$$

Three filters were studied based on different assumptions about the noise. The first filter is referred to as the signal-modulated colored (SMC) noise filter (Eq. (1.15)), with the assumption that the effective noise term is signal-modulated and colored (non-white). The second filter (Eq. (1.16)) assumes the noise is signal-modulated but white (the SMW filter). The last filter is the signal-independent white (SIW) noise filter. The results shows that the SMC filter was generally superior to the SMW and SIW filters.

Optimal Estimators Based on Bayesian Approach

The model that includes both signal-dependent and signal-independent noise is given by

$$r = s + kf(s)n_1 + n_2 \tag{1.18}$$

Optimal estimators for the above noise model are derived by Froehlich [14], which, as expected, have more complicated expressions than that for the classical case of signal-independent noise. Due to the mathematical complexity of these estimators, various suboptimal estimators were purposed in [17]. The six estimators, with the first three being optimal and the rest suboptimal, are summarized in Table 1.1:

1. Minimum mean square error (MMSE)
2. Maximum *a posterior* probability (MAP)
3. Maximum likelihood (ML)
4. Weighted spatial averaging (WSA)
5. Modified signal-independent MAP (MSIMAP)
6. James-Stein (JS)

One characteristic shared by the MMSE, MAP, and ML estimators is computational complexity. It is generally undesirable to integrate numerically at every pixel,

Estimator	Expression
MMSE	$\hat{s}_{MMSE} = \int_{-\infty}^{\infty} sp(s\|r)ds$
MAP	solution of $a\hat{s}_{MAP}^3 + b\hat{s}_{MAP}^2 + c\hat{s}_{MAP} + d = 0$ where a, b, c, and d are functions of $k, \sigma_1^2, \sigma_2^2$, and μ_s.
ML	$\hat{s}_{ML} = \left[r^2 + \left(\frac{k^2\sigma_1^2}{2}\right)^2 + \frac{2\sigma_2^2}{k^2\sigma_1^2}r + \left(\frac{\sigma_2^2}{k^2\sigma_1^2}\right)^2\right]^{1/2} - \frac{k^2\sigma_1^2}{2} - \frac{\sigma_2^2}{k^2\sigma_1^2}$
WSA	$\hat{s}_{WSA} = \bar{r} = \frac{1}{(2N+1)^2}\sum_{i=-N}^{N}\sum_{j=-N}^{N} r$ within a moving window of size (2N+1) x (2N+1)
MSIMAP	$\hat{s}_{MSIMAP} = \frac{\sigma_s^2}{\sigma_s^2+\sigma_2^2}r + \frac{\sigma_2^2}{\sigma_s^2+\sigma_2^2}\bar{r}$ within a moving window of size (2N+1) x (2N+1), σ_s^2 is known
JS	$\hat{s}_{JS} = \bar{r} + (1 - \frac{\sigma_2^2}{\sigma_r^2})(r - \bar{r})$ within a moving window of size (2N+1) x (2N+1), σ_r^2 is estimated

Table 1.1: Summary of different estimators. The quantities σ_r^2, σ_s^2, σ_1^2, and σ_2^2 are the variances of r, s, n_1, and n_2 respectively. Mean of the signal s is designated μ_s.

just as it is undesirable to solve a polynomial at every pixel. To sacrifice some theoretical performance for ease of implementation, adaptive suboptimal estimators were proposed and were found to perform slightly worse than optimal estimators. If the original image contains a lot of fine detail, i.e. high-frequency content, the WSA estimator should not be used because it is essentially a lowpass filter.

1.3.2 Generalized Homomorphic Transformation

A different approach to process images degraded by signal-dependent film grain noise is to perform a pointwise transformation whose purpose is to transform the noise into approximately signal independent additive Gaussian noise. From the noise model in Eq. (1.8), the nonlinear coupling of signal noise makes linear filtering not very attractive. Therefore, decouplng of the noise from the signal is highly desirable. This is obtained by passing the observed image r through a memoryless nonlinearity $g(r)$,

such that:

$$g(r) = g(s + kf(s)n) = t(s) + N(n) \tag{1.19}$$

where $t(s)$ is a nonlinear function of s and $N(n)$ is a signal-dependent noise term. Once this is done, conventional filtering techniques for additive signal-independent noise can be employed. The sequence of operations is shown in Fig 1.2.

It was shown in [39] that the only type of signal-dependent noise that can be decoupled exactly (and hence signal-independent) by $g(r)$ is the multiplicative noise. In the case of speckle noise (a type of multiplicative noise), a logarithmic transformation was shown to transform the noise into additive and signal-independent, with its probability density distribution becomes approximately Gaussian [18]. In cases where it is desired to have variance of the noise independent of the signal, Arsenault and Denis [19, 20, 21] derived a generalized transformation for signal-dependent noise of arbitrary form. Consider a noisy image r with film grain noise having a probability distribution $p(r)$. Since the noise is signal-dependent, the standard deviation of r is a known function of the mean value μ_r, and so we can write

$$\sigma_r = H(\mu_r) \tag{1.20}$$

where $H(\cdot)$ represents the signal-dependence functionality of σ_r. The objective here is to find a transformation

$$w = g(r) \tag{1.21}$$

such that $w = g(r)$ will contain constant-variance noise over a wide range of image values. The mean of the variable w is equal to

$$\bar{w} = \int_{-\infty}^{\infty} g(r)p(r)dr \tag{1.22}$$

Figure 1.2: Block diagram showing the sequence of operations employing homomorphic transformation.

Expanding the function $g(r)$ into a Taylor series about the mean μ_r gives

$$\bar{w} = \int_{-\infty}^{\infty} \sum_{n=0}^{\infty} \frac{g^{(n)}(\mu_r)}{n!}(r-\mu_r)^n p(r)dr. \tag{1.23}$$

Similarily the variance is given by

$$\sigma_w^2 = \int_{-\infty}^{\infty} \left[\sum_{n=0}^{\infty} \frac{g^{(n)}(\mu_r)}{n!}(r-\mu_r)^n\right]^2 p(r)dr - \overline{g(r)}^2 + \ldots \tag{1.24}$$

Integrating the above expression term by term, and setting the variance to a constant K^2, with the assumption that the terms of order higher than the first are negligible gives

$$\sigma_w = K = g^{'}(\mu_r)\sigma_r = g^{'}(\mu_r)H(\mu_r). \tag{1.25}$$

The solution to this differential equation is obviously

$$g(r) = w = K\int \frac{dr}{H(r)} \tag{1.26}$$

For any signal-dependent noise, once the relationship between the variance and the signal has been determined, the above formula can be used to find a transformation that will make the variance of the noise additive and signal independent. With the noise model in Eq. (1.8) at a given pixel (x, y), we have

$$\mu_r = E[r(x,y)] = s(x,y) \tag{1.27}$$

$$\sigma_r = k\sigma_n s^p(x,y) = k\mu_r^p = H(\mu_r) \tag{1.28}$$

for $\sigma_n^2 = 1$. It then follows that

$$H(r) = kr^p \tag{1.29}$$

Substituting Eq. (1.29) into Eq. (1.26) and integrating gives

$$w = \frac{Kr^{1-p}}{k(1-p)} \tag{1.30}$$

For the typical case of $p = 0.5$, the above expression becomes

$$w = \frac{2K\sqrt{r}}{k} \tag{1.31}$$

and transforms the signal-dependent noise into additive signal independent noise with variance K^2.

Accuracy of the Transformation

To determine the accuracy of the transformation $w = g(r)$, w can be expanded into a Taylor series about s as:

$$\begin{aligned} w &= \frac{K}{k(1-p)}[s + ks^p n]^{1-p} \\ &= \frac{K}{k(1-p)}s^{1-p}[1 + ks^{p-1}n]^{1-p} \\ &= \frac{K}{k(1-p)}s^{1-p}\left[1 + \frac{(1-p)(-p)}{2}k^2 s^{2(p-1)}n^2 + \ldots\right] \end{aligned} \tag{1.32}$$

Using a similiar procedure to compute the variance σ_w^2 gives [21]

$$\sigma_w^2 = K^2\left[1 + \frac{p(2+3p)}{2}k^2 s^{2(p-1)} + \frac{p(1+p)^2(9+7p)}{6}k^4 s^{4(p-1)} + \ldots\right] \tag{1.33}$$

The first order estimate of the error on the variance, assuming negligible higher order terms, is

$$\Delta\sigma_w^2 = \frac{K^2 p(2+3p)}{2}k^2 s^{2(p-1)} \tag{1.34}$$

thus the relative error is written as

$$\epsilon = \frac{\Delta\sigma_w^2}{\sigma_w^2} = \frac{p(2+3p)}{2}k^2 s^{2(p-1)} \tag{1.35}$$

With the following typical values of parameters for photographic film [21]

$$k^2 = 0.01 \qquad p = 0.5 \tag{1.36}$$

and $\epsilon < 10\%$, the range of s must be greater than 0.09, which is usually the case in practice. This shows that the transformation can be used over a wide range of signal densities.

Applications

For extraction of information from images corrupted by signal-dependent noise, generalized homomorphic transformation can be combined with numerous techniques

developed for signal-independent noise. This approach has the advantage that it allows the application of conventional image processing techniques on images corrupted by signal-dependent noise without sacrificing performance. The price to pay is the additional step of pre-processing the data.

Experiments were carried out by Arsenault and Denis [13] to perform Wiener filtering on film grain noise. The image was first transformed to make the noise additive and signal-independent, and then followed by Wiener filtering, where the transformed quantities were used. Local-statistics processing combined with homomorphic transformation was done by Arsenault and Levesque [12] to process images degraded by film grain noise and by multiplicative noise. It was found that filtering designed for signal-independent noise combined with homomorphic transformation produced better results.

1.4 Motivations of the Thesis

Over the past years research has been conducted on suppressing film grain noise. The signal-dependence of the noise has been considered and specific noise filtering techniques were developed. These techniques only employ second-order statistics of the image. Because photographic images are usually non-Gaussian, and film grain noise is nonlinearly related to the signal, higher-order statistics (H.O.S.) offers a new signal processing tool that can capture the non-Gaussian information in the image. Furthermore, the noise is usually assumed signal-dependent Gaussian, but virtually no work has been reported on under what circumstances this assumption is valid. The nature of the noise distribution will affect the choice of filtering schemes to be used. Moreover, existing techniques only concentrate on removing images corrupted by signal-dependent noise, but not the reverse process: film grain noise generation. Since images photographed on film contain a characteristic look that is different from images generated by a computer or photographed by video, accurate noise generation has applications in television and motion picture productions, as digitized film images are routinely combined with computer generated images into one frame. Artificial

noise must be added in order for the result to appear realistic. Based on the above, the motivations of this research are the following:

1. Determine under what circumstances do the assumption on film grain noise being Gaussian is valid. Knowledge on the nature of noise distribution is desired.
2. Investigate new filtering techniques that are based on H.O.S. for grayscale and eventually to color images.
3. Develop techniques for film grain noise generation for applications in television and motion picture productions.

1.5 Contributions of the Thesis

The major contributions of this thesis are listed below:

1. By extracting actual film grain noise and computing its variance and higher-order statistics, some deviation from Gaussianity was observed. The noise distribution was modeled as a generalized Gaussian distribution and its parameters were estimated. Nevertheless, over a practical range of signals film grain noise was observed to exhibit Gaussian behavior. This material is presented in Chapter 2.
2. A higher-order statistics based filter is introduced in filtering signal-dependent film grain noise. This filter employs H.O.S. of the image and minimizes a H.O.S. based criterion. It was found that the proposed filter performed better than existing one that used second-order statistics by 1 dB (in SNR) on average in both high and low SNR cases. Moreover, a new method for estimating noise parameters using second and higher-order statistics is described. These are discussed in Chapter 3.

3. By using the generalized homomorphic transformation, a local-statistics based filtering algorithm is proposed in Chapter 4. This new filter has excellent edge preservation and selective noise smoothing properties. The proposed filter can be applied in grayscale and color images corrupted with signal-dependent film grain noise. On average this new filter outperformed existing local-statistics based filters by 1 dB (in SNR) for grayscale images and resulted in 12% less error (in L_2 norm) for color images.

4. Using the proposed local-statistics based filter and the noise parameter estimation method, realistic film grain noise generation for grayscale and color images by matching the higher-order statistics of the noise was studied. The noise-added image and the original noisy image were similar in visual appearance and in their noise level.

Conclusions of this research, as well as future directions, are summarized in Chapter 5. Detailed derivations of some results are given in the Appendix.

Chapter 2

Review of H.O.S. and Investigation on Film Grain Noise

To test the validity of the noise model, some experimental work on extracting actual film grain noise was carried out. In particular, the assumption that film grain noise is Gaussian with signal-dependent variance was investigated. Once the noise is extracted, statistics of the noise as well as properties of the noise distribution can be computed. The noise distribution is modeled by the three-parameter generalized Gaussian density, and parameters of this distribution are then estimated. This chapter is organized as follows. First a short review of higher-order statistics (H.O.S.) and the parametric generalized Gaussian distribution (GGD) are provided, then results of actual film grain noise statistics are presented.

2.1 Review of H.O.S.

Higher-order statistics, also known as cumulants, are closely related to the more familiar moments and can be expressed in terms of them. For example, the familiar

first and second moments are the mean and variance, respectively, whereas the second-order cumulant is the variance itself. One attractive property of H.O.S. is that all kth-order cumulants of Gaussian processes are identically equal to zero for $k > 2$. By working with cumulants of order greater than two, extraction of non-Gaussian signals from Gaussian signals is possible. Moreover, another attractive property of cumulants is that the cumulant of the sum of two statistcally independent random processes is the sum of the cumulants of the individual processes. It is therefore very convenient to work with cumulants than with moments, which do not have that property.

The following serves as a brief overview of definitions and properties of H.O.S.

2.1.1 Definitions and Properties

Given a collection of n random variables, $x = [y_1, y_2, \ldots y_n]^T$, the n-th order cumulants of the random variables is defined as: [22]

$$C[y_1, \ldots, y_n] = (-j)^n \frac{\partial_n \ln E exp(j\mathbf{v}^T\mathbf{y})}{\partial v_1 \ldots \partial v_n}|_{v_1=\ldots=v_n=0} \tag{2.1}$$

where $\mathbf{v} = [v_1, \ldots, v_n]^T$. For zero-mean real random variables, the nth order stationary random process $\{x(t)\}$, the 2nd, 3rd, and 4th order cumulants are given by

$$C_{2,x}(\tau) = E\{x(t)x(t+\tau)\} \tag{2.2}$$

$$C_{3,x}(\tau_1, \tau_2) = E\{x(t)x(t+\tau_1)x(t+\tau_2)\} \tag{2.3}$$

$$\begin{aligned} C_{4,x}(\tau_1, \tau_2, \tau_3) = E\{x(t)x(t+\tau_1)x(t+\tau_2)x(t+\tau_3)\} \\ - C_{2,x}(\tau_1)C_{2,x}(\tau_2 - \tau_3) \\ - C_{2,x}(\tau_2)C_{2,x}(\tau_3 - \tau_1) \\ - C_{2,x}(\tau_3)C_{2,x}(\tau_1 - \tau_2). \end{aligned} \tag{2.4}$$

The quantities $c_2^x = C_{2,x}(0)$, $c_3^x = C_{3,x}(0,0)$, $c_4^x = C_{4,x}(0,0,0)$ are known as variance, skewness, and kurtosis respectively. Assuming that the n-th order cumulant is absolutely summable, the n-th order polyspectrum is defined as the $(n-1)$-dimensional

discrete Fourier transform of the n-th order cumulant: [22]

$$S_{n,x}(\omega_1,\ldots,\omega_{n-1}) = \sum_{\tau_1=-\infty}^{\infty} \cdots \sum_{\tau_{n-1}=-\infty}^{\infty} C_{n,x}(\tau_1,\ldots,\tau_{n-1}) exp\Big[-j\sum_{i=1}^{n-1}\omega_i\tau_i\Big] \qquad (2.5)$$

In the case of continuous-time signals, the above Fourier transform is replaced by the multidimensional Fourier transform. For $n = 2$, $S_{2,x}$ is the well-known power spectrum; for $n = 3$, $S_{3,x}$ is called the bispectrum; and for $n = 4$, $S_{4,x}$ is known as the trispectrum.

Following is a list of some important properties of cumulants: [22], [23]

1. If $c_1,\ldots,c_n$ are constants, and $y_1,\ldots,y_n$ are random variables, then:

$$cum(c_1y_1,\ldots,c_ny_n) = \Big(\prod_{i=1}^{n} c_i\Big) cum(y_1,\ldots,y_n) \qquad (2.6)$$

2. Given the random variables $x_0, y_0, z_1,\ldots,z_n$, cumulants of sums equal sums of cumulants:

$$cum(x_0+y_0,z_1,\ldots,z_n) = cum(x_0,z_1,\ldots,z_n) + cum(y_0,z_1,\ldots,z_n) \qquad (2.7)$$

3. If $(i_1,\ldots,i_n)$ is a permutation of $(1,\ldots,n)$, then cumulants are symmetric in their arguments:

$$cum(x_1,\ldots,x_n) = cum(x_{i1},\ldots,x_{in}) \qquad (2.8)$$

4. If c is a constant, then

$$cum(c+x_1,x_2,\ldots,x_n) = cum(x_1,\ldots,x_n) \qquad (2.9)$$

5. If the random process $\{y(i)\}$ is independent identically distributed (i.i.d.), then

$$C_{y,n}(\tau_1,\ldots,\tau_{n-1}) = \gamma_{y,n}\delta(\tau_1)\ldots\delta(\tau_{n-1}) \qquad (2.10)$$

where $\delta(\tau)$ is the delta function.

6. If the random variables $\{x_i\}$ are independent of the random variable $\{y_i\}$, then

$$cum(x_1 + y_1, \ldots, x_k + y_k) = cum(x_1, \ldots, x_k) + cum(y_1, \ldots, y_k) \tag{2.11}$$

7. If a subset of the n random variables $\{y_i\}$ is independent of the rest, then

$$cum(y_1, \ldots, y_k) = 0 \tag{2.12}$$

2.2 The Parametric Generalized Gaussian Distribution

The parametric generalized Gaussian distribution (GGD) is a distribution that is closely related to the more familiar Gaussian distribution. This parametric family of distribution is obtained by generalizing the Gaussian distribution to obtain a variable rate of exponential decay ρ. It has the following form: [24, 25]

$$f(x) = \frac{1}{2\Gamma(1 + 1/\rho)A(\rho)} \, exp\left(-\frac{|x - \mu|}{A(\rho)}\right)^{\rho} \tag{2.13}$$

where

$$A(\rho) = \sqrt{\frac{\sigma^2\Gamma(1/\rho)}{\Gamma(3/\rho)}}, \tag{2.14}$$

$\Gamma(\cdot)$ is the gamma function, σ^2 is the variance, and μ is the mean of the distribution. Note that $\rho = 1$ gives the Laplacian distribution function, and $\rho = 2$ gives the familiar Gaussian distribution. The three parameter values are such that

$$0 < \rho, \sigma^2 < \infty \quad and \quad -\infty < \mu < \infty \tag{2.15}$$

Note that for $0 < \rho < 1$ the distribution has more heavy tails, while as $\rho \to \infty$, the distribution becomes more uniform.

2.3 Extraction of Actual Noise Statistics

To acquire actual film grain noise data, it is desirable to scan an uniformly exposed and developed print. In other words, the ideal image in this case has a constant value throughout. Assuming the light source to be purely uniform, and measurement noise being negligible, any fluctuations in the digitized output image are due to film grain noise. The noise extraction procedure is shown in Fig. 2.1

From the signal-dependent film grain noise model, it can be observed that the noise variance is directly proportional to the mean of the signal μ_r (assuming $p = 0.5$), in this case a constant:

$$\sigma^2_{noise} \propto \mu_r \tag{2.16}$$

Images with different uniform color were photographed using Canon AF35MII camera, with Kodak Gold ASA 400 film. The developed prints were then digitized using Canon IX-4025 digital image scanner at a resolution of 300 dpi (dots per inch). This resolution was used simply because it is commonly used in practice. For a constant signal, the noise model predicts that the variance of the noise is linearly related to the signal, the skewness and kurtosis are identically zero. Relationships between noise variance and signal mean for red, green, and blue channels are plotted in Fig. 2.2. For comparsion, skewness and kurtosis of the noise are also included.

From the figures, some trends are observed:

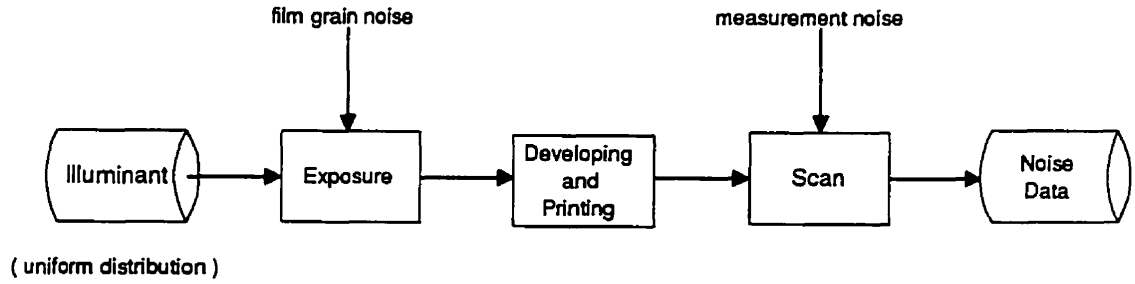

Figure 2.1: Procedure for noise extraction.

- The noise variance increases with the signal, and therefore signal dependency of film grain noise is observed. It appears that the relationship between noise variance and signal is linear, as least for density levels smaller than 1, as predicted by the noise model for $p = 0.5$.

- For signals with relatively low densities ($\mu_r < 1$), film grain noise increased steadily. However, as signals are greater than one, a larger rate of increase for film grain noise variance is observed. This may suggest that at high densities, the noise model is inadequate in describing the observed pheonomenon.

- Higher-order statistics of film grain noise are relatively small at low signal densities, but are substantially large at high signal densities. This indicates that the assumption of Gaussian film grain noise may not be valid under those situations.

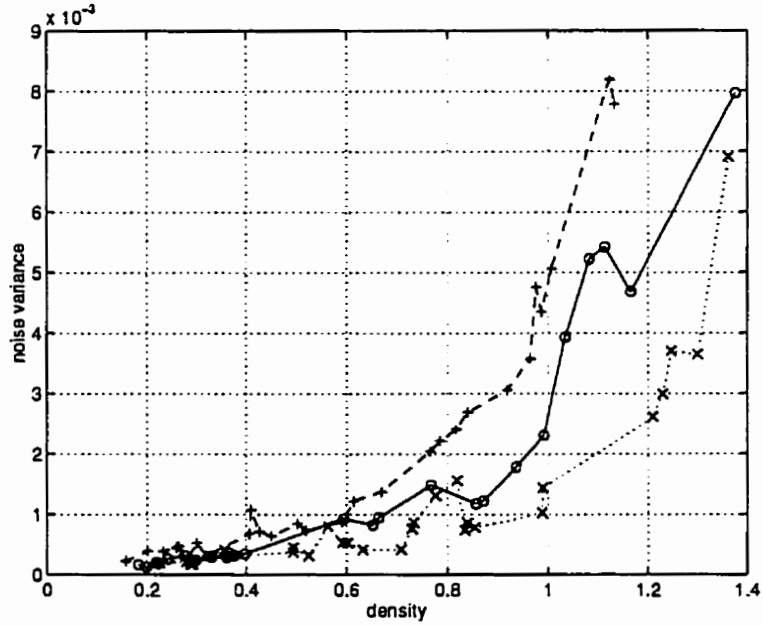

Figure 2.2: Relationship between noise variance and signal for different channels. Data for red channel are shown with 'o', green channel with 'x', and blue channel with '+'.

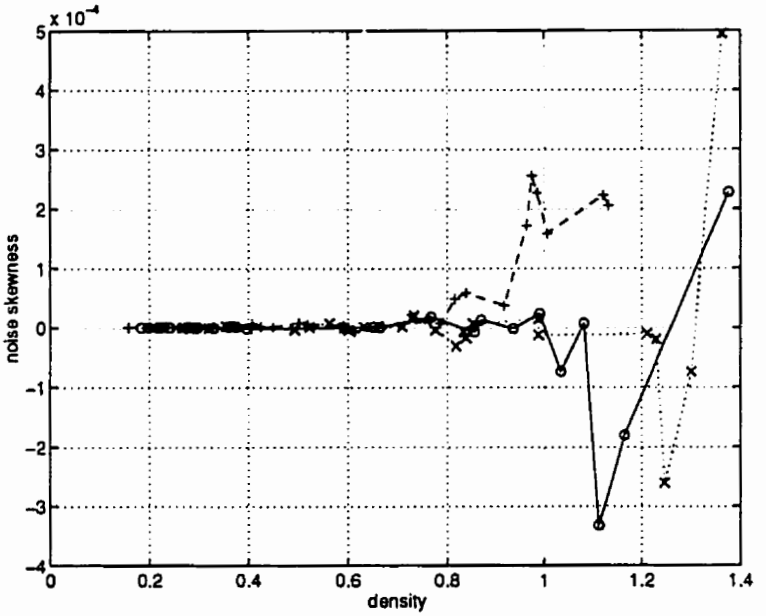

Figure 2.3: Relationship between noise skewness and signal for different channels. Data for red channel are shown with 'o', green channel with 'x', and blue channel with '+'.

2.4 Determination of the Parameters for the GGD

From the last section, it is observed that at low signal densities the noise model works well, while at high densities the rate of increase for noise variance is higher. Moreover, the skewness and kurtosis of film grain noise are large. These suggest that the Gaussian assumption about the noise may not be valid at high densities. In this section, the generalized Gaussian distribution (GGD) is assumed. Parameters for this noise distribution are estimated over the range of the signal.

There are three parameters in the GGD, the mean μ, variance σ^2, and rate of exponential decay ρ. The mean and variance are estimated using sample averaging for an image r of size M x N:

$$\mu = \frac{1}{MN} \sum_{i=1}^{M} \sum_{j=1}^{N} r(i,j) \tag{2.17}$$

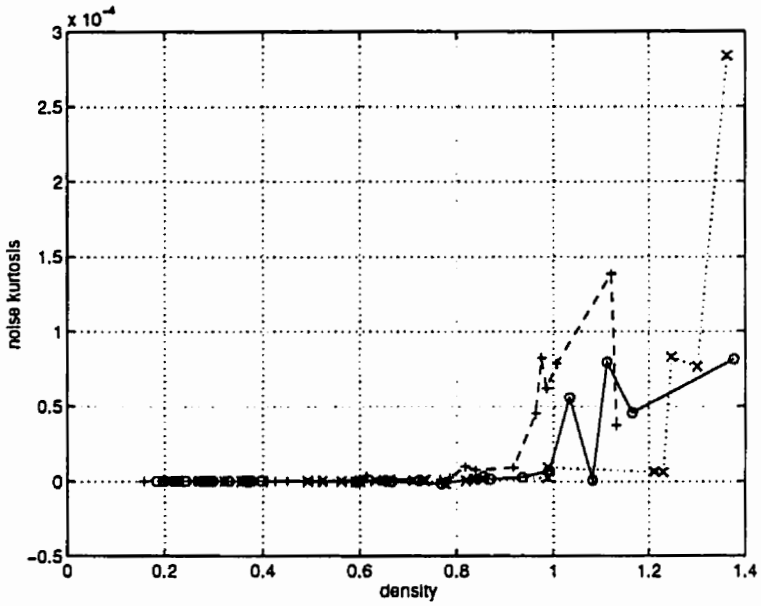

Figure 2.4: Relationship between noise kurtosis and signal for different channels. Data for red channel are shown with 'o', green channel with 'x', and blue channel with '+'.

and

$$\sigma^2 = \frac{1}{MN}\sum_{i=1}^{M}\sum_{j=1}^{N} r^2(i,j) - \mu^2 \tag{2.18}$$

The parameter ρ is obtained by selecting the ρ that results in the minimum mean square error. The procedure to determine ρ is to first select the range $1 \leq \rho \leq 3$ in increments of 0.1. Then for each value of ρ compute the mean square error between the actual noise distribution and the GGD. The value of ρ desired is the one having the minimum mean square error. This procedure is repeated for each channel. Noise histogram with the estimated GGD are plotted in Figs. 2.5 - 2.7. Results of estimation of ρ are summarized in Table 2.1.

It is clear from the Table that as signal density increases, the assumption on Gaussian film grain noise may not be valid. The noise becomes more impulsive in nature. The observation may be explained by noting that a very high signal density in the print means a small optical energy detected by film grains. Under those circumstances

only a small number of silver halide grains are converted to silver during development, and hence the Central Limit Theorem may not apply. Nonetheless, over a practical range of signal densities film grain noise is observed to be Gaussian.

	Estimated ρ with signal density of range:			
Channel	0.25-0.28	0.48-0.55	0.76-0.78	1.10-1.15
red	2.1	1.9	1.9	1.7
green	2.1	2.1	1.9	1.5
blue	2.1	2.0	2.1	1.7

Table 2.1: Estimated parameter ρ of the GGD for different channels.

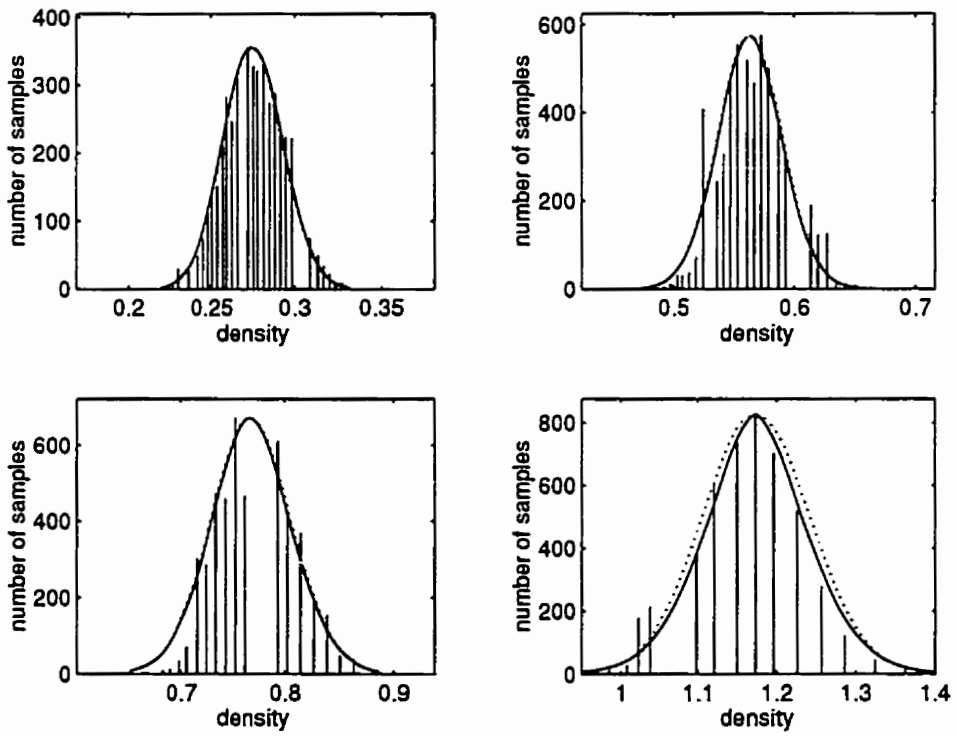

Figure 2.5: Noise histogram of the red channel. The dotted curve is the Gaussian distribution while the solid curve is the estimated GGD.

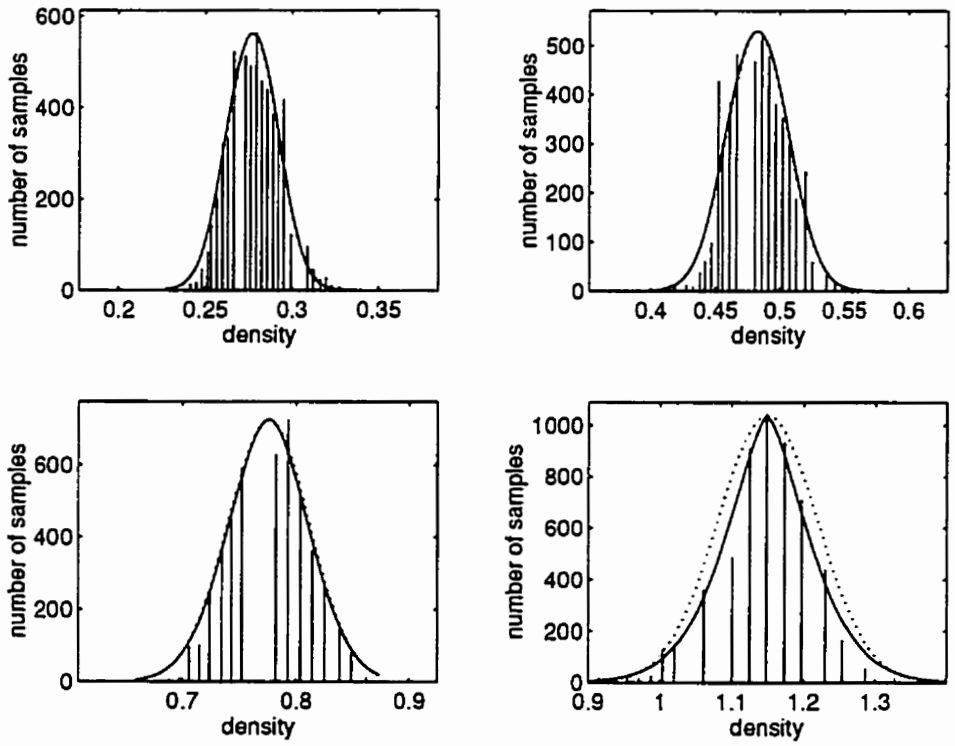

Figure 2.6: Noise histogram of the green channel. The dotted curve is the Gaussian distribution while the solid curve is the estimated GGD.

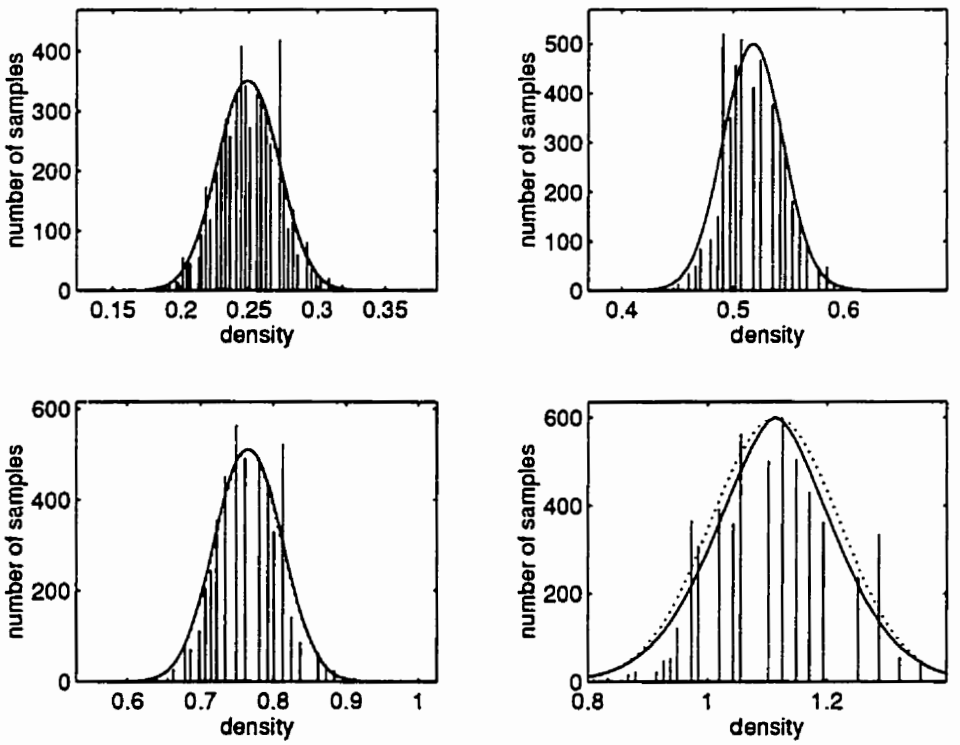

Figure 2.7: Noise histogram of the blue channel. The dotted curve is the Gaussian distribution while the solid curve is the estimated GGD.

Chapter 3

Film Grain Noise Removal Based on Higher-Order Statistics

In this chapter, use of higher-order statistics (H.O.S.) in film grain noise removal is considered. Because photographic images are highly non-Gaussian and film grain noise is nonlinearly related to the original image, a lot more information can be extracted from their higher-order statistics, and filtering schemes based on H.O.S. can give better performance. Moreover, in the presence of Gaussian measurement noise, higher-order statistics of the observed image would contain contributions from the non-Gaussian image and signal-dependent film grain noise only, which allows more reliable estimation of film grain noise parameters.

3.1 Film Grain Noise Model

The image model used for film grain noise is the additive signal-modulated noise model described in Chapter 1: [10, 11, 12, 13]

$$r(x,y) = s(x,y) + ks^p(x,y)n(x,y) \tag{3.1}$$

where s is the noiseless image measured in density, and r is the observed image. The above noise model does not include a signal-independent noise term which accounts for measurement noise. If this noise term is added, the above model becomes:

$$r(x,y) = s(x,y) + ks^p(x,y)n(x,y) + w(x,y) \tag{3.2}$$

with ks^pn being signal-dependent noise, and w being the signal-independent noise. The range of k and p are:

$$k > 0 \quad and \quad 0.2 \leq p \leq 0.7 \tag{3.3}$$

where a typical value of 0.5 is held for p. Assumptions made above are:

- Film grain noise is a Gaussian process. Furthermore, film grain noise is a white noise in the sense that density measurements in different spatial positions in photographic film are statistically uncorrelated provided the samples are spaced farther apart than the grain size of the film. Thus, the noise term n is *i.i.d.* Gaussian with zero mean and unit variance ($\sigma_n^2 = 1$).
- Measurement noise w is Gaussian (colored or white) with zero mean and unknown variance σ_w^2.
- The ideal image s, noise terms n, and w, are statistically independent of each other.

3.2 Design of Higher-Order Statistics Based Filter

Assuming the proposed filter $h(x,y)$ be a finite impulse response (FIR) filter with a support region of

$$h(x,y) \neq 0 \qquad for \qquad a \leq x \leq b, c \leq y \leq d, \tag{3.4}$$

the filter coefficients $h(x,y)$ can be solved by minimizing a higher-order statistics criterion that is an extension of the mean square error (MSE) criterion used in the

correlation based Wiener filter. Let the error signal $e(x,y)$ be defined as:

$$e(x,y) = s(x,y) - \sum_{i=a}^{b}\sum_{j=c}^{d} h(i,j)r(x-i,y-j). \tag{3.5}$$

the proposed filter $h(x,y)$ is designed by minimizing the following criterion [27]:

$$J_C^M(h) = \left\{ \sum_{\alpha=-\infty}^{\infty}\sum_{\beta=-\infty}^{\infty} Cum^M(e_{xy}, e_{xy}, r_{x-\alpha,y-\beta}, \ldots, r_{x-\alpha,y-\beta}) \right\}^2 \geq J_C^M(\hat{h}) \tag{3.6}$$

with $e_{xy} = e(x,y)$ and $\hat{h}(x,y)$ being the optimum filter based on the cumulant based criterion J_C^M.

3.2.1 Cumulant-Based Wiener-Hopf Equation

To compute the optimum filter coefficients, we can extend the correlation based Wiener-Hopf equation and the orthogonality principle to higher-order statistics. It is well known that the correlation based Wiener-Hopf equation has the form:

$$R_{rs}(\alpha,\beta) = \sum_{i=a}^{b}\sum_{j=c}^{d} h(i,j)R_{rr}(\alpha-i,\beta-j), \tag{3.7}$$

where R_{rs} is the cross correlation of the observed and ideal images. The above equation can be obtained by the orthogonality principle, which states that:

$$E[e(x,y)r(x,y)] = 0. \tag{3.8}$$

Analogously, by using a cumulant based orthogonality principle, a cumulant based Wiener-Hopf equation can be derived. By using the idea described in [28], let $\tilde{h}(x,y)$ be the filter satisfying the following cumulant based orthogonality condition:

$$\sum_{\alpha=-\infty}^{\infty}\sum_{\beta=-\infty}^{\infty} Cum^M(e_{xy}, r_{x-i,y-j}, r_{x-\alpha,y-\beta}, \ldots, r_{x-\alpha,y-\beta}) = 0 \tag{3.9}$$

where $a \leq i \leq b, c \leq j \leq d$ is the support region of the optimum filter. Then it can

be shown that $\tilde{h}$ is the optimum filter associated with the criterion J_C^M (for detailed derivation see Appendix). Thus we have for $h_{ij} = \tilde{h}_{ij}$,

$$J_{Cmin}^M = \Big\{ \sum_\alpha \sum_\beta Cum^M(\tilde{e}_{xy}, s_{xy}, r_{x-\alpha,y-\beta}, \ldots, r_{x-\alpha,y-\beta}) \Big\}^2 \tag{3.10}$$

To derive the cumulant based Wiener-Hopf equation, we start with the orthogonality condition (Eq. (3.9)), and substitute the expression for $e(x,y)$ into Eq. (3.9):

$$\begin{aligned}
\sum_{\alpha=-\infty}^{\infty} \sum_{\beta=-\infty}^{\infty} Cum^M(e_{xy}, r_{x-i,y-j}, r_{x-\alpha,y-\beta}, \ldots, r_{x-\alpha,y-\beta}) &= 0 \\
= \sum_\alpha \sum_\beta Cum^M(s_{xy} - \sum_{k=a}^{b} \sum_{l=c}^{d} h_{kl} r_{x-k,y-l}, r_{x-i,y-j}, r_{x-\alpha,y-\beta}, \ldots, r_{x-\alpha,y-\beta}) & \\
= \sum_\alpha \sum_\beta Cum^M(s_{xy}, r_{x-i,y-j}, r_{x-\alpha,y-\beta}, \ldots, r_{x-\alpha,y-\beta}) & \\
- \sum_{k=a}^{b} \sum_{l=c}^{d} h_{kl} \sum_\alpha \sum_\beta Cum^M(r_{x-k,y-l}, r_{x-i,y-j}, r_{x-\alpha,y-\beta}, \ldots, r_{x-\alpha,y-\beta}) = 0 &
\end{aligned}$$

$$\Rightarrow C_{sr}(p,q) = \sum_{i=a}^{b} \sum_{j=c}^{d} h(i,j) C_{rr}(p-i, q-j) \tag{3.11}$$

where C_{sr} and C_{rr} are defined as

$$C_{sr}(i,j) = \sum_{\alpha=-\infty}^{\infty} \sum_{\beta=-\infty}^{\infty} Cum^M(s_{xy}, r_{x-i,y-j}, r_{x-\alpha,y-\beta}, \ldots, r_{x-\alpha,y-\beta}) \tag{3.12}$$

$$C_{rr}(i,j) = \sum_{\alpha=-\infty}^{\infty} \sum_{\beta=-\infty}^{\infty} Cum^M(r_{xy}, r_{x-i,y-j}, r_{x-\alpha,y-\beta}, \ldots, r_{x-\alpha,y-\beta}) \tag{3.13}$$

The above derivation can be applied similarly to moments, i.e., moment based criterion leading to a moment based orthogonality condition and a moment based Wiener-Hopf equation. The corresponding criterion to be minimized now and the orthogonality condition are

$$J_M^M(h) = \Big\{ \sum_{\alpha=-\infty}^{\infty} \sum_{\beta=-\infty}^{\infty} Mom^M(e_{xy}, e_{xy}, r_{x-\alpha,y-\beta}, \ldots, r_{x-\alpha,y-\beta}) \Big\}^2 \geq J_M^M(\hat{h}) \tag{3.14}$$

and

$$\sum_{\alpha=-\infty}^{\infty}\sum_{\beta=-\infty}^{\infty} Mom^{M}(e_{xy}, r_{x-i,y-j}, r_{x-\alpha,y-\beta}, \ldots, r_{x-\alpha,y-\beta}) \;=\; 0$$

which lead to another HOS-based Wiener-Hopf equation:

$$M_{sr}(p,q) = \sum_{i=a}^{b}\sum_{j=c}^{d} h(i,j) M_{rr}(p-i, q-j) \tag{3.15}$$

with

$$M_{sr}(i,j) = \sum_{\alpha=-\infty}^{\infty}\sum_{\beta=-\infty}^{\infty} Mom^{M}(s_{xy}, r_{x-i,y-j}, r_{x-\alpha,y-\beta}, \ldots, r_{x-\alpha,y-\beta}) \tag{3.16}$$

$$M_{rr}(i,j) = \sum_{\alpha=-\infty}^{\infty}\sum_{\beta=-\infty}^{\infty} Mom^{M}(r_{x,y}, r_{x-i,y-j}, r_{x-\alpha,y-\beta}, \ldots, r_{x-\alpha,y-\beta}) \tag{3.17}$$

3.2.2 Estimation of Higher-Order Statistics

The use of Eqs. (3.11) and (3.15) requires that C_{sr}, C_{rr}, M_{sr}, and M_{rr} are known. In practice, higher-order cumulants and moments are estimated by replacing the expectation operator by sample averaging over the data. Estimation of C_{rr} and M_{rr} can be done since we have access to the observed signal. However, C_{sr} and M_{sr} are not easy to obtain unless we know the signal exactly, which is impossible. Thus it is important to determine their relationships with the original signal statistics C_{ss} and M_{ss}, which are assumed known.

By substituting the noise model (Eq. (3.1)) into the definitions of C_{rr} and C_{sr}, we have for $M = 3$ and $p = 0.5$:

$$C_{rr}(i,j) = C_{sr}(i,j) + k^2(R_s(i,j) - \mu_s^2) + k^2 \sum_{\alpha}\sum_{\beta}(R_s(\alpha,\beta) - \mu_s^2)\delta(i,j) \tag{3.18}$$

and

$$C_{sr}(i,j) = \sum_{\alpha}\sum_{\beta} Cum(s_{xy}, s_{x-i,y-j}, s_{x-\alpha,y-\beta}) + k^2(R_s(i,j) - \mu_s^2) \tag{3.19}$$

Similarly,

$$M_{rr}(i,j) = M_{sr}(i,j) + k^2 R_s(i,j) + k^2 \sum_{\alpha} \sum_{\beta} R_s(\alpha,\beta)\delta(i,j) \tag{3.20}$$

and

$$M_{sr}(i,j) = \sum_{\alpha} \sum_{\beta} Mom(s_{xy}, s_{x-i,y-j}, s_{x-\alpha,y-\beta}) + k^2 R_s(i,j) \tag{3.21}$$

where R_s and μ_s are the autocorrelation and the mean of the signal s respectively:

$$R_s(i,j) = E[s(x,y)s(x-i,y-j)] \tag{3.22}$$

To estimate the sample moment for an image of size M x N, the following estimator is used:

$$Mom(r_{xy}, r_{x-i,y-j}, r_{x-\alpha,y-\beta}) = \frac{1}{MN} \sum_{\alpha} \sum_{\beta} \sum_{x=1}^{M} \sum_{y=1}^{N} r_{xy} r_{x-i,y-j} r_{x-\alpha,y-\beta} \tag{3.23}$$

The third-order cumulant is related to the third-order moment through the following:

$$\begin{aligned} Cum(r_{xy}, r_{x-i,y-j}, r_{x-\alpha,y-\beta}) \;=\; & Mom(r_{xy}, r_{x-i,y-j}, r_{x-\alpha,y-\beta}) \\ & -\mu_r R_r(i-\alpha, j-\beta) \\ & -\mu_r R_r(\alpha,\beta) \\ & -\mu_r R_r(i,j) + 2\mu_r^2 \end{aligned} \tag{3.24}$$

Note from the definitions of M_{rr} and C_{rr} that the range of α and β is from negative infinity to positive infinity. In practice this is impossible, hence a smaller range must be used. Through experimentation a good compromise between the number of computations (speed) and performance is the range:

$$-2 \leq \alpha \leq 2 \quad and \quad -2 \leq \beta \leq 2 \tag{3.25}$$

3.3 Parameter Estimation

The calculations of Eqs. (3.18) and (3.19) require that the constant k be known. However, when this information is not available, we must estimate the constant from

the observed image statistics and the *a prior* ideal image statistics. In the case of signal-dependent noise only, the variance, skewness, and kurtosis of the received image are related to that of the original image by the following equations:

$$\sigma_r^2 = \sigma_s^2 + k^2 E[s^{2p}] \tag{3.26}$$

$$c_3^r = c_3^s + 3k^2(E[s^{2p+1}] - E[s]E[s^{2p}]) \tag{3.27}$$

$$\begin{aligned} c_4^r &= c_4^s + 6k^2 E[s^{2p+2}] + 3k^4 E[s^{4p}] - 12k^2 E[s]E[s^{2p+1}] \\ &\quad -6k^2 E[s^2]E[s^{2p}] - 3k^4 E^2[s^{2p}] + 12k^2 E^2[s]E[s^{2p}] \end{aligned} \tag{3.28}$$

with c_3^r and c_4^r representing the skewness and kurtosis of the observed image respectively. In the special case of $p = 0.5$, the above relationships can be simplified to:

$$\sigma_r^2 = \sigma_s^2 + k^2 E[s] \tag{3.29}$$

$$c_3^r = c_3^s + 3k^2\sigma_s^2 \tag{3.30}$$

$$c_4^r = c_4^s + 6k^2 c_3^r - 15k^4\sigma_s^2 \tag{3.31}$$

Similarly, for both signal-dependent and signal-independent Gaussian noises, with $p = 0.5$, we have:

$$\sigma_r^2 = \sigma_s^2 + k^2 E[s] + \sigma_w^2 \tag{3.32}$$

$$c_3^r = c_3^s + 3k^2\sigma_s^2 \tag{3.33}$$

$$c_4^r = c_4^g + 6k^2 c_3^r - 15k^4 \sigma_s^2 \tag{3.34}$$

The value of k can then be solved by substituting the statistics of the observed image (which can be estimated) and the *a prior* image statistics (σ_s^2, c_s^3, and c_s^4) into any of the above equations. Note from the above equations that the use of higher-order statistics in the presence of Gaussian measurement noise leads to better estimation of k, as cumulants of Gaussian noise are identically zero.

3.4 Simulation Results

In this section, the above proposed methods in estimation of the parameter k, and signal-dependent film grain noise removal based on H.O.S. are applied. Four test images of size 256 x 256 are used: Lenna, Peppers, Melon, and Mountain. They are shown in Fig. 3.1 - 3.4.

3.4.1 Results on Parameter Estimation

To test the validity of parameter estimation of k, a number of simulations were performed for the following two cases:

- signal-dependent noise only
- mixture of signal-dependent/signal-independent noise

Signal-dependent film grain noise and Gaussian measurement noise are added to the image 'Lenna'. Sample cumulants are calculated using the following relationships:

$$c_1^r = m_1^r \tag{3.35}$$

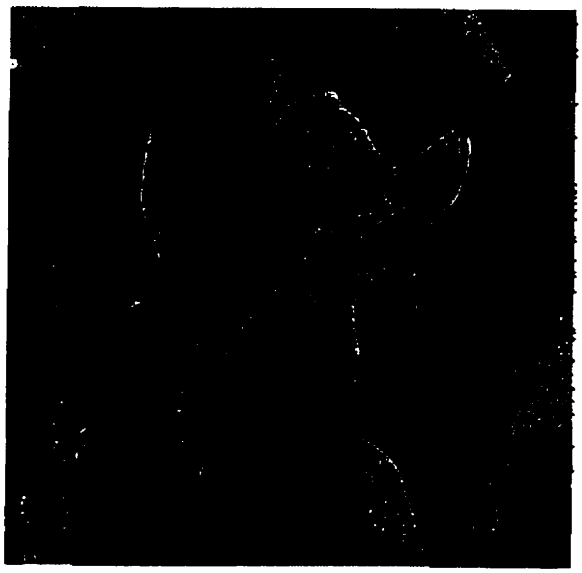

Figure 3.1: Test image: 'Lenna'.

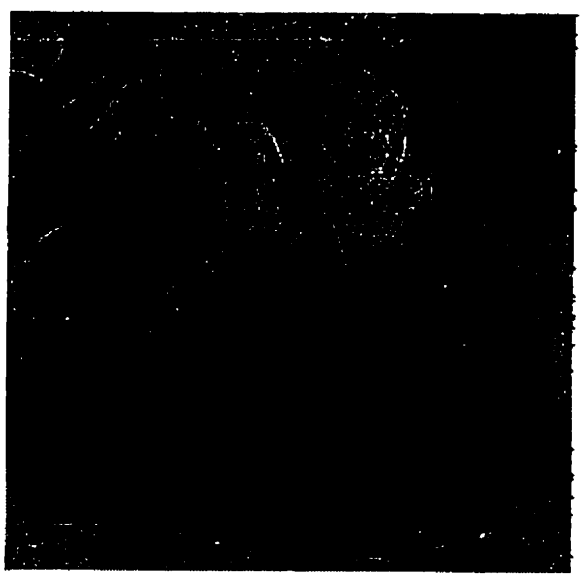

Figure 3.2: Test image: 'Peppers'.

Figure 3.3: Test image: 'Melon'.

Figure 3.4: Test image: 'Mountain'.

$$c_2^r = \sigma_r^2 = m_2^r - (m_1^r)^2 \tag{3.36}$$

$$c_3^r = m_3^r - 3m_1^r m_2^r + 2(m_1^r)^2 \tag{3.37}$$

$$c_4^r = m_4^r - 4m_1^r m_3^r - 3(m_2^r)^2 + 12(m_1^r)^2 m_2^r - 6(m_1^r)^4 \tag{3.38}$$

The quantities m_1^r, m_2^r, m_3^r, and m_4^r are estimated from an M x N image using sample averaging:

$$m_1^r = \frac{1}{MN} \sum_{x=1}^{M} \sum_{y=1}^{N} r(x,y) \tag{3.39}$$

$$m_2^r = \frac{1}{MN} \sum_{x=1}^{M} \sum_{y=1}^{N} r^2(x,y) \tag{3.40}$$

$$m_3^r = \frac{1}{MN} \sum_{x=1}^{M} \sum_{y=1}^{N} r^3(x,y) \tag{3.41}$$

$$m_4^r = \frac{1}{MN} \sum_{x=1}^{M} \sum_{y=1}^{N} r^4(x,y) \tag{3.42}$$

The signal statistics σ_s^2, c_3^s, and c_4^s of the image 'Lenna' are known *a prior* and are used to solve for k. The parameter p was fixed to be 0.5 throughout the experiments since this is typical for a variety of film stocks. Because the variance of the signal-independent noise is assumed unknown, k is solved using Eq. (3.29). Two values of k were selected, and correspond to moderate and severe noise corruption:

$$k = 0.1 \quad and \quad k = 0.2 \tag{3.43}$$

The value of k determines the degree of degradation, as can be seen from the variance of the signal-dependent noise term:

$$\sigma^2_{noise} = k^2\sigma^2_s \tag{3.44}$$

Fifty independent runs were performed, with the results summarized below.

	estimated k (mean± standard deviation):		
σ^2_w	2nd order statistics	3rd order statistics	4th order statistics
0	0.0999±0.0015	0.0999±0.0024	0.0998±0.0033
0.05	0.1299±0.0014	0.1003±0.0030	0.1006±0.0041
0.10	0.1939±0.0013	0.1013±0.0039	0.1009±0.0072
0.15	0.2681±0.0015	0.1004±0.0058	0.1007±0.0082
0.20	0.3465±0.0014	0.0990±0.0096	0.0984±0.0159

Table 3.1: Estimation of k with true value k=0.1.

	estimated k (mean± standard deviation):		
σ^2_w	2nd order statistics	3rd order statistics	4th order statistics
0	0.1998±0.0013	0.1995±0.0027	0.1996±0.0064
0.05	0.2162±0.0017	0.1997±0.0035	0.2011±0.0080
0.10	0.2596±0.0016	0.1997±0.0042	0.2007±0.0082
0.15	0.3195±0.0012	0.2003±0.0035	0.2005±0.0112
0.20	0.3876±0.0017	0.1995±0.0055	0.2037±0.0209

Table 3.2: Estimation of k with true value k=0.2.

The advantage of using H.O.S. in estimation is evident from the tables. Second-order statistics results in high bias and low variance, whereas estimation using H.O.S. has low bias but higher variance. It is clear that estimating k using H.O.S. is better than using second-order statistics in the presence of Gaussian measurement noise.

3.4.2 Results on Noise Filtering

For noise filtering, again two different cases were investigated:

- signal-dependent noise only
- mixture of signal-dependent/signal-independent noise

The value of p for signal-dependent noise was held to be 0.5 in all cases. For signal-dependent noise only two different values of k were used ($k = 0.1$ and $k = 0.2$) to determine the effect of noise on the performance. For a mixture of signal-dependent and signal-independent noise, only the value $k = 0.1$ was selected. Variance of measurement noise σ_w^2 is chosen to be 0.005.

Four test images, shown in Figs. 3.1 - 3.4, were used in the simulations. The criteria used in evaluating the performance were 1) signal-to-noise ratio (SNR), 2) mean absolute error (MAE), and 3) mean square error (MSE) which is similar to SNR. All the criteria were calculated in the density domain. These are defined below for an image of size M x N:

$$\text{SNR (in dB)} = 10 \log_{10} \frac{\sum_{x=0}^{M-1} \sum_{y=0}^{N-1} s^2(x,y)}{\sum_{x=0}^{M-1} \sum_{y=0}^{N-1} [\hat{s}(x,y) - s(x,y)]^2} \tag{3.45}$$

$$\text{MAE} = \frac{1}{MN} \sum_{x=0}^{M-1} \sum_{y=0}^{N-1} [\hat{s}(x,y) - s(x,y)] \tag{3.46}$$

$$\text{MSE} = \frac{1}{MN} \sum_{x=0}^{M-1} \sum_{y=0}^{N-1} [\hat{s}(x,y) - s(x,y)]^2 \tag{3.47}$$

where s and $\hat{s}$ are the ideal and estimated images, respectively. Two filter sizes were chosen in this simulation: 3 x 3 and 5 x 5. Although using filters with a larger size (e.g. 7 x 7 or 9 x 9) would improve performance, they tend to smear the edges (boundaries or contours at which a significant change in pixel value occurs) in the image which are pleasing to the eye, thus smaller filter sizes were selected. Wiener filter designed based on the usual correlation based criterion [10] (designated M_2) and

the two proposed higher-order statistics based criteria (third-order moment M_3 and third-order cumulant C_3) are compared. Results are summarized in Tables 3.3 -3.14. Filtered Lenna using different filters are depicted in Figs. 3.6 - 3.8.

A number of observations can be made:

- The performance of higher-order moment based filter is comparable to that using the usual correlation based criterion in all cases. On average higher-order moment based filter achieved better SNR than the correlation based filter by 1 dB. This improvement may be due to the fact that more information about the image statistics was utilized. In the case of third order statistics, both third order moment and correlation of the original image (see Eq. (3.21)) were used.

- The cumulant based filter performed as good as the higher-order moment and correlation based filters in the case of signal-dependent noise only. However, for a mixture of film grain noise and measurement noise, the cumulant based filter is not suitable. By examining the cumulant based Wiener-Hopf equation in Eq. (3.11):

$$C_{sr}(p,q) = \sum_{i=a}^{b}\sum_{j=c}^{d} h(i,j)C_{rr}(p-i,q-j) \tag{3.48}$$

  we have for a mixture of noise:

$$\begin{aligned} C_{sr}\ (\ mixture\ of\ noise\ ) &\approx C_{sr}\ (\ film\ grain\ noise\ only\ ) \\ and\ \ C_{rr}\ (\ mixture\ of\ noise\ ) &\approx C_{rr}\ (\ film\ grain\ noise\ only\ ) \end{aligned} \tag{3.49}$$

  thus the cumulant based criterion cannot not recognize the Gaussian measurement noise. The filter performed as if only film grain noise is present.

- Performance of cumulant based filter depends heavily on the properties of the image. For third-order cumulant, if the distribution of an image is close to Gaussian or is symmetric, then it is not appropriate to use the cumulant based filter, because images with those properties have zero third-order cumulant. Table 3.15 shows the skewness, as well as the mean and variance, of the four

images. It can be observed that the image 'Mountain' has the lowest skewness, thus third-order cumulant based filter did not perform well in that case. If fourth-order cumulant is used, the filter should perform well in the case of film grain noise only, as indicated in Table 3.16.

- For severe noise conditions, a filter size of 5 x 5 has a better noise suppression than a filter size of 3 x 3, as expected. Moreover, the effect of blurring for large filter size is not noticeable with size 5 x 5. Thus, in employing H.O.S. based filters this filter size is recommended for severe noise corruption.

3.4.3 Computational Complexity

In this section, the complexity issue of the proposed H.O.S. based filters is discussed. In particular, the number of multiplications involved for different filters is considered, since multiplication is the most costly arithmetic operation in terms of time. We can find the total number of multiplications for each filter, but since the only difference for these filters is the choice of signal statistics, we only need to compute the number of multiplications in estimating signal statistics.

For correlation based Wiener filter, the mean estimator of the autocorrelation for an M x N image is:

$$R_{rr}(i,j) = \frac{1}{MN} \sum_{x=1}^{M} \sum_{y=1}^{N} r(x,y) r(x-i, y-j). \tag{3.50}$$

The number of multiplications involved is approximately (MN). For third-order moment, the mean estimator has the form:

$$M_{rr}(i,j) = \frac{1}{MN} \sum_{\alpha=-2}^{2} \sum_{\beta=-2}^{2} \sum_{x=1}^{M} \sum_{y=1}^{N} r(x,y) r(x-i, y-j) r(x-\alpha, y-\beta) \tag{3.51}$$

whereas for third-order cumulant the number of multiplications required is of the same order as that of the third-order moment. Using a direct approach would end up having approximately $50(MN)$ multiplications for third-order moment. Thus the approximate number of multiplications for correlation based and third-order statistics

based methods are (MN) and $50(MN)$ respectively.

The above analysis may discourage the use of H.O.S. based algorithms because of the higher computational load. However, there exists fast algorithms for estimating higher-order statistics of the signals which speeds up computational time. As proposed in [31], expression for estimating third-order moment can be separated into two parts: $r(x,y)r(x-i,y-j)$ and $r(x-\alpha,y-\beta)$, one depends on (i,j) and the other on (α,β), so that the first part can be calculated and stored in memory for different values of (α,β). From the results in [31] the number of multiplications saved using this method was 50%. With efficient methods in estimating signal statistics, combined with the advance of computing technology, it is becoming less of a concern for computational complexity.

	SNR (dB)		MAE		MSE	
filter size	3x3	5x5	3x3	5x5	3x3	5x5
unfiltered	16.7591	16.7591	4.6375e-2	4.6375e-2	3.6820e-3	3.6820e-3
M_2	19.8458	19.8822	3.1849e-2	3.1466e-2	1.8089e-3	1.7938e-3
M_3	19.9902	19.9891	3.1212e-2	3.1075e-2	1.7498e-3	1.7502e-3
C_3	20.1143	19.2769	3.0150e-2	3.2913e-2	1.7005e-3	2.0621e-3

Table 3.3: Test image 'Lenna' with signal-dependent noise only (k=0.1).

	SNR (dB)		MAE		MSE	
filter size	3x3	5x5	3x3	5x5	3x3	5x5
unfiltered	10.8349	10.8349	9.2195e-2	9.2195e-2	1.4405e-2	1.4405e-2
M_2	16.5937	16.7553	4.5936e-2	4.4621e-2	3.8250e-3	3.6853e-3
M_3	16.7243	16.9639	4.5027e-2	4.3277e-2	3.7117e-3	3.5125e-3
C_3	16.8165	16.8867	4.4157e-2	4.2889e-2	3.6337e-3	3.5755e-3

Table 3.4: Test image 'Lenna' with signal-dependent noise only (k=0.2).

	SNR (dB)		MAE		MSE	
filter size	3x3	5x5	3x3	5x5	3x3	5x5
unfiltered	13.0270	13.0270	7.3938e-2	7.3938e-2	8.6957e-3	8.6957e-3
M_2	17.7796	17.8305	4.1604e-2	4.0966e-2	2.9110e-3	2.8771e-3
M_3	17.8464	17.9216	4.1266e-2	4.0651e-2	2.8666e-3	2.8174e-3
C_3	13.7575	15.1257	6.7819e-2	5.7488e-2	7.3494e-3	5.3632e-3

Table 3.5: Test image 'Lenna' with mixture of signal-dependent noise (k=0.1) and measurement noise ($\sigma_w^2 = 0.005$).

	SNR (dB)		MAE		MSE	
filter size	3x3	5x5	3x3	5x5	3x3	5x5
unfiltered	15.9961	15.9961	4.0384e-2	4.0384e-2	2.7924e-3	2.7924e-3
M_2	19.6853	19.8014	2.5401e-2	2.4801e-2	1.1941e-3	1.1627e-3
M_3	19.7162	19.7003	2.5293e-2	2.5244e-2	1.1857e-3	1.1900e-3
C_3	19.4486	17.3086	2.6396e-2	3.3160e-2	1.2610e-3	2.0641e-3

Table 3.6: Test image 'Peppers' with signal-dependent noise only (k=0.1).

	SNR (dB)		MAE		MSE	
filter size	3x3	5x5	3x3	5x5	3x3	5x5
unfiltered	10.0312	10.0312	8.0373e-2	8.0373e-2	1.1027e-3	1.1027e-3
M_2	16.4570	16.6923	3.6344e-2	3.4806e-2	2.5112e-3	2.3788e-3
M_3	16.4925	16.6979	3.6170e-2	3.4857e-2	2.4908e-3	2.3757e-3
C_3	16.3785	16.5459	3.6990e-2	3.5781e-2	2.5570e-3	2.4603e-3

Table 3.7: Test image 'Peppers' with signal-dependent noise only (k=0.2).

	SNR (dB)		MAE		MSE	
filter size	3x3	5x5	3x3	5x5	3x3	5x5
unfiltered	11.5534	11.5534	6.9966e-2	6.9966e-2	7.7668e-3	7.7668e-3
M_2	17.2267	17.3699	3.4643e-2	3.3724e-2	2.1034e-3	2.0352e-3
M_3	17.1175	17.1662	3.5386e-2	3.5062e-2	2.1569e-3	2.1329e-3
C_3	15.6441	13.1576	4.3338e-2	5.6770e-2	3.0281e-3	5.3682e-3

Table 3.8: Test image 'Peppers' with mixture of signal-dependent noise (k=0.1) and measurement noise ($\sigma_w^2 = 0.005$).

	SNR (dB)		MAE		MSE	
filter size	3x3	5x5	3x3	5x5	3x3	5x5
unfiltered	15.8383	15.8383	3.9878e-2	3.9878e-2	2.7628e-3	2.7628e-3
M_2	20.7981	20.9273	2.2272e-2	2.1968e-2	8.8181e-4	8.5595e-4
M_3	21.1387	20.8048	2.1377e-2	2.2191e-2	8.1529e-4	8.8044e-4
C_3	21.5274	20.4498	1.9827e-2	2.3291e-2	7.4549e-4	9.55458e-4

Table 3.9: Test image 'Melon' with signal-dependent noise only (k=0.1).

	SNR (dB)		MAE		MSE	
filter size	3x3	5x5	3x3	5x5	3x3	5x5
unfiltered	9.9375	9.9375	7.8637e-2	7.8637e-2	1.0751e-3	1.0751e-3
M_2	17.5055	17.9161	3.2525e-2	3.1050e-2	1.8820e-3	1.7123e-3
M_3	17.6681	18.0810	3.1941e-2	3.0408e-2	1.8129e-3	1.6485e-3
C_3	17.8314	18.2453	3.1111e-2	2.9176e-2	1.7460e-3	1.5873e-3

Table 3.10: Test image 'Melon' with signal-dependent noise only (k=0.2).

	SNR (dB)		MAE		MSE	
filter size	3x3	5x5	3x3	5x5	3x3	5x5
unfiltered	8.5227	8.5227	9.6386e-2	9.6386e-2	1.4891e-3	1.4891e-3
M_2	16.5695	17.3293	3.7451e-2	3.4009e-2	2.3347e-3	1.9600e-3
M_3	16.6166	17.3538	3.7313e-2	3.3833-2	2.3095e-3	1.9490e-3
C_3	16.0607	14.0968	3.9314e-2	4.9320e-2	2.6249e-3	4.1257e-3

Table 3.11: Test image 'Melon' with mixture of signal-dependent noise (k=0.1) and measurement noise ($\sigma_w^2 = 0.005$).

	SNR (dB)		MAE		MSE	
filter size	3x3	5x5	3x3	5x5	3x3	5x5
unfiltered	15.9772	15.9772	4.5280e-2	4.5280e-2	3.4005e-3	3.4005e-3
M_2	20.9042	21.0538	2.5644e-2	2.5126e-2	1.0936e-3	1.0565e-3
M_3	21.6888	21.4412	2.1905e-2	2.3844e-2	9.1283e-4	9.6637e-4
C_3	20.7989	15.5664	2.3356e-2	4.7584e-2	1.1204e-3	3.7379e-3

Table 3.12: Test image 'Mountain' with signal-dependent noise only (k=0.1).

	SNR (dB)		MAE		MSE	
filter size	3x3	5x5	3x3	5x5	3x3	5x5
unfiltered	9.9872	9.9872	9.0280e-2	9.0280e-2	1.3507e-3	1.3507e-3
M_2	17.5884	17.9846	3.7456e-2	3.5580e-2	2.3465e-3	2.1419e-3
M_3	17.8750	18.5062	3.6073e-2	3.2963e-2	2.1967e-3	1.8995e-3
C_3	17.8997	16.6623	3.5422e-2	3.7131e-2	2.1842e-3	2.9042e-3

Table 3.13: Test image 'Mountain' with signal-dependent noise only (k=0.2).

	SNR (dB)		MAE		MSE	
filter size	3x3	5x5	3x3	5x5	3x3	5x5
unfiltered	12.1036	12.1036	7.2457e-2	7.2457e-2	8.2966e-3	8.2966e-3
M_2	18.8252	18.9651	3.3124e-2	3.2495e-2	1.7650e-3	1.7091e-3
M_3	19.1878	19.3845	3.1541e-2	3.0633-2	1.6236e-3	1.5517e-3
C_3	14.1962	11.3033	5.6995e-2	7.9364e-2	5.1244e-3	9.9755e-3

Table 3.14: Test image 'Mountain' with mixture of signal-dependent noise (k=0.1) and measurement noise ($\sigma_w^2 = 0.005$).

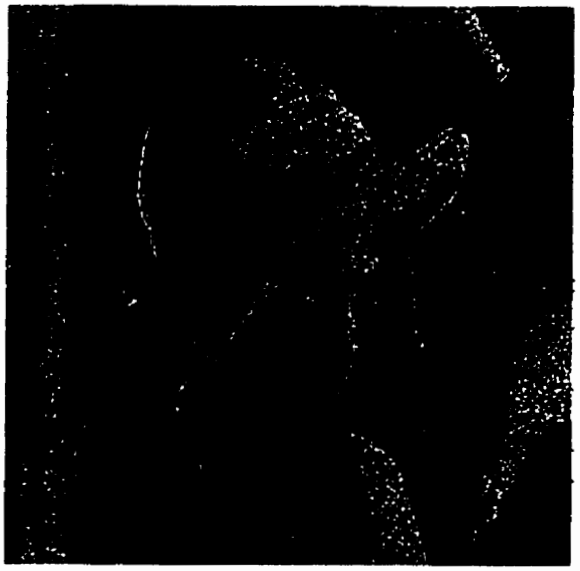

Figure 3.5: Corrupted Lenna (k=0.1).

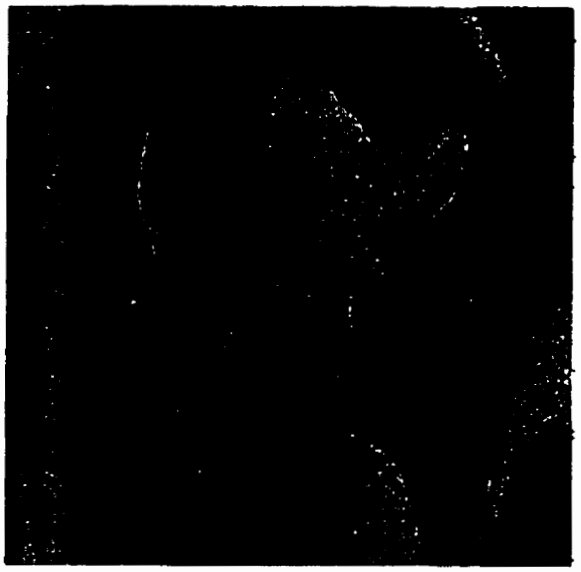

Figure 3.6: Lenna filtered by the correlation-based filter.

Figure 3.7: Lenna filtered by third-order moment based filter.

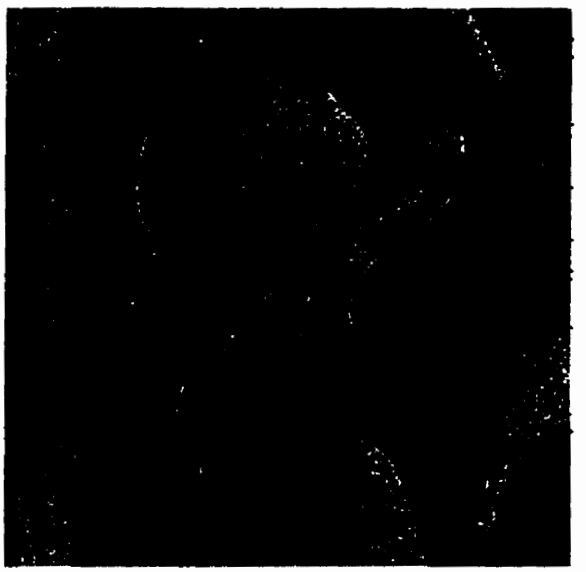

Figure 3.8: Lenna filtered by third-order cumulant based filter.

	Image Statistics		
Image	mean	variance	skewness
Lenna	3.6363e-1	4.2353e-2	7.2266e-3
Peppers	2.7942e-1	3.2994e-2	1.1394e-2
Melon	2.7426e-1	3.0751e-2	8.8570e-3
Mountain	3.3807e-1	2.0373e-2	1.0025e-3

Table 3.15: Image statistics of various test images.

	SNR (dB)		MAE		MSE	
filter size	3x3	5x5	3x3	5x5	3x3	5x5
unfiltered	15.9772	15.9772	4.5280e-2	4.5280e-2	3.4005e-3	3.4005e-3
M_2	20.9042	21.0538	2.5644e-2	2.5126e-2	1.0936e-3	1.0565e-3
M_4	21.5968	21.3010	2.2600e-2	2.2631e-2	9.3237e-4	9.9807e-4
C_4	21.7648	21.7349	2.2393e-2	2.2608e-2	8.9398e-4	9.0317e-4

Table 3.16: Performance of fourth-order cumulant based filter with test image 'Mountain'. The value of k is held to be 0.1.

Chapter 4

Generalized Homomorphic Adaptive Filtering

Because of the computational load of the H.O.S. based filter, a more efficient filter is desired. In this chapter a new nonlinear adaptive filtering technique is described. The first step in the removal of film grain noise is to apply the generalized homomorphic transformation, which approximately decouples the noise from the signal. Since film grain noise is signal-dependent and Gaussian, using the generalized homomorphic transformation to stablize its variance and utilizing second-order statistics only may be sufficient. A linear adaptive filtering operation utilizing the local-statistics of the image then takes place, and is followed by an inverse transformation. This proposed technique belongs to a class of contrast enhancement techniques and can be extended to multivariate signals, i.e. color images. First, the generalized homomorphic transformation is revisited, then the proposed filter is discussed. This filter can be combined with the technique developed in Chapter 3 to estimate the noise parameter for film grain noise generation. The correct amount of artificial film grain noise can be added to the ideal image to match any film pattern for applications in television and motion picture productions.

4.1 Generalized Homomorphic Transformation

From Chapter 1, the generalized homomorphic transformation $g(r)$ has the following form [19, 20, 21]:

$$g(r) = w = K \int \frac{dr}{H(r)} \tag{4.1}$$

where $\sigma_r = H(\mu_r)$ is the standard deviation of the noisy image r and $\mu_r = E[r(x,y)] = s(x,y)$ is the mean value for the noise model:

$$r(x,y) = s(x,y) + ks^p(x,y)n(x,y) \tag{4.2}$$

The above expression assumes negligible measurement noise because in many practical cases the main source of degradation for photographic images is film grain noise only. With Eq. (4.2) we have for $p = 0.5$:

$$g(r) = \frac{2K\sqrt{r}}{k} \tag{4.3}$$

The transformed image model (for $K = 1$) then becomes [29]

$$w = g(r) \approx g(s) + n = u + n \tag{4.4}$$

Notice the noise in the transformed domain is approximately additive Gaussian and signal-independent.

It is interesting to see the effect of a square-root operation on the corrupted signal in Eq. (4.2). Ignoring the proportionality constant $(2K/k)$ in the transformation (Eq. (4.3)), the output of this nonlinear system can be approximated as a Taylor expansion of $g(r)$ about s with an order M:

$$\begin{aligned}
\sqrt{r} &= \{s + k\sqrt{s}n\}^{1/2} \\
&= \sqrt{s}\left\{1 + \frac{kn}{\sqrt{s}}\right\}^{1/2} \\
&= \sqrt{s}\left\{1 + \sum_{m=1}^{M} \binom{1/2}{m} \left(\frac{kn}{\sqrt{s}}\right)^m\right\} \\
&= \sqrt{s} + X
\end{aligned} \tag{4.5}$$

The above expression is of the familiar form with noiseless signal $\sqrt{s}$ and 'additive' noise X, where X is defined as:

$$X = \sum_{m=1}^{M} \binom{1/2}{m} (kn)^m s^{(1-m)/2} \tag{4.6}$$

Since the value of k is less than unity, and the order of the magnitude for the ratio $(n/\sqrt{s})$ is normally of 1, a small Taylor expansion of order M is sufficient. For example, with an order of $M = 4$, X takes the form:

$$X = \frac{1}{2}kn + \binom{1/2}{2} \frac{1}{\sqrt{s}} k^2 n^2 + \binom{1/2}{3} \frac{k^3 n^3}{s} + \binom{1/2}{4} k^4 n^4 s^{-3/2} \tag{4.7}$$

It is observed that even for the second term the order of magnitude is smaller than that for the first term. Thus contributions from higher order terms are negligible compared with the first one. When only the signal-independent first term of X is retained, the noise variance becomes (assuming n is zero mean, unit variance Gaussian):

$$\sigma_X^2 = k^2/4 \tag{4.8}$$

If, in addition, $\sqrt{r}$ is multiplied by the proportionality constant $2/k$ in the transformation, then the resulting noise variance (assuming higher order terms are negligible) becomes the variance of n, namely

$$\sigma_X^2 = \sigma_n^2 = 1 \tag{4.9}$$

4.2 Generalized Homomorphic Adaptive Filtering

From the transformed image model (additive signal-independent Gaussian noise), we see that conventional linear filtering techniques can be applied. Example of a classical linear filter is the Wiener filter, which takes a 'global' view of the image statistics and applies the same fixed filter to the entire image. In this way noise is smoothed, but some details are also destroyed. Or in another case edges are preserved well, but noise in uniform regions may not be smoothed sufficiently. The objective here is to adjust filter coefficients accordingly such that less smoothing is performed

when near the edge and more smoothing when away from edge. One class of filters that showed some success in edge preservation and selective noise smoothing is the contrast enhancement filters [30, 33, 34]. These techniques consider a 'local' rather than 'global' view of image statistics to determine signal activity in different regions in order to minimize the blurring effect and at the same time smooth noise. The general approach is to separate the image into two parts: lowpass and highpass components. A scaled version of the highpass component, whose weight is determined by the local-statistics of image, is usually added back to the filtered image to enhance its contrast. Thus, based on this approach, the proposed filter has the form:

$$\hat{u} = h * w + a(w - h * w) \tag{4.10}$$

where $\hat{u}$ is the estimate of the ideal image u, w is the corrupted image after transforming r, * denotes 2-d convolution, a is a signal-adaptive variable constrained to have a value between 0 and 1:

$$0 \leq \ a \ \leq 1 \tag{4.11}$$

and h is a filter mask defined as a weighted window of size $(2N+1)$ x $(2N+1)$ on the current pixel (x, y). Interpretation of this filter is described in section 4.2.1. Using the concept developed in [32], the filter mask h is expressed as:

$$h(i,j) = exp\left(-\frac{(w(i,j) - w(x,y))^2}{b^2}\right) \tag{4.12}$$

The idea used here is to calculate the filter coefficients through a discriminating function (in this case a Gaussian function) that tends to 1 for pixels having value similar to that of the current pixel, and tends to 0 for the others. The first term in Eq. (4.10) can be interpreted as a low frequency component, whereas the last term a high frequency component. To determine the adaptive variable a, we can optimize it by minimizing the mean square error (MSE). Denoting

$$h(w) = h * w \tag{4.13}$$

the criterion to be minimized is:

$$MSE = E[(u - \hat{u})^2] \tag{4.14}$$

with u is the ideal image after transforming s. After simplification (for derivation see Appendix), we have

$$\begin{aligned} a_{optimum} &= \frac{E[u^2] + E[h^2(w)] - 2E[uh(w)]}{E[u^2] + E[n^2] + E[h^2(w)] - 2E[uh(w)]} \\ &= \frac{E[w^2] - E[n^2] + E[h^2(w)] - 2E[uh(w)]}{E[w^2] + E[h^2(w)] - 2E[uh(w)]} \end{aligned} \tag{4.15}$$

For ease of computation, a sub-optimal solution can be obtained by treating the first term $h * w$ as the sample mean, and therefore a has the form

$$a_{sub\_optimum} = \frac{\sigma_u^2(x,y)}{\sigma_u^2(x,y) + \sigma_n^2(x,y)} \tag{4.16}$$

By definition σ_n^2 has a value of unity, thus we can further simplify the above equations to

$$a_{optimum} = \frac{E[w^2] + E[h^2(w)] - 2E[uh(w)] - 1}{E[w^2] + E[h^2(w)] - 2E[uh(w)]} \tag{4.17}$$

$$a_{sub\_optimum} = \frac{\sigma_w^2(x,y) - 1}{\sigma_w^2(x,y)} \tag{4.18}$$

The variable b in Eq. (4.12) which controls the slope of the discriminating Gaussian function is left as a design parameter. Through experimentation a good choice for b is the value σ_w.

4.2.1 Interpretation of the Filter

The proposed filter can be interpreted as a combination of lowpass and highpass component as depicted in Fig. 4.1. The lowpass component is the first term $h * w$, while the highpass component is the difference between the corrupted image w and its lowpass component $h * w$, weighted by a nonstationary variable a. The filter mask h in the lowpass component is a function of the differences between the current pixel

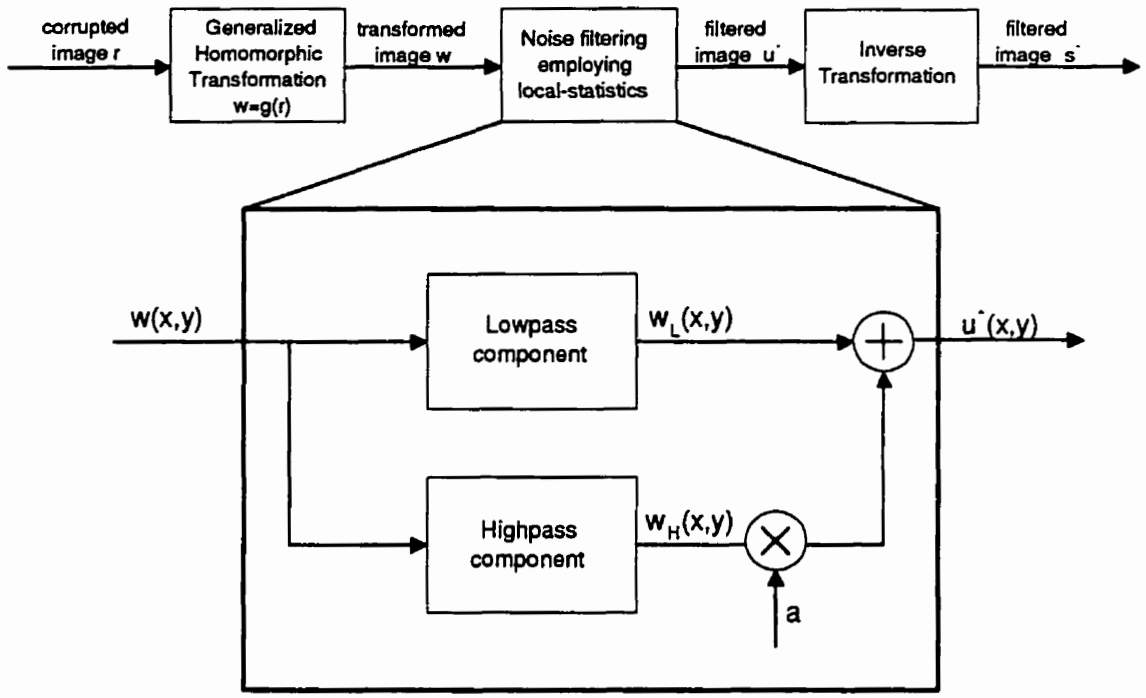

Figure 4.1: Adaptive noise smoothing filter structure.

(i, j) and other pixels within the moving window. If the pixels are widely different, which corresponds to a large pixel distance $|w(i, j) - w(x, y)|$, the estimated lowpass pixel value will put more weight on the current pixel. The parameter b in the filter mask further controls the width of the Gaussian curve, and is taken the value σ_w. If the variance is high, which corresponds to a large b and may indicate a high level of noise, the slope of the Gaussian function is small. This results in more smoothing of pixels. However, if the variance is low, then more emphasis is on edge preservation.

To further understand the filter structure, Eq. (4.10) can be rearranged as:

$$\hat{u} = (1 - a)(h * w) + aw \tag{4.19}$$

In this form the filter output is seen as a weighted sum of the lowpass component of the observation $w(x, y)$ and the observation itself. To selectively smooth noise and preserve edge, the parameter a is allowed to be nonstationary to minimize local mean square error. In situations where the signal-to-noise ratio (SNR) is high, the estimate

$\hat{u}$ puts more weight on the observation to preserve edges. On the other hand, when the SNR is low, the filter outputs the lowpass version of the observation because the observation is too noisy.

4.2.2 Computation of Local Statistics

The computation of the parameter a in Eq. (4.15) requires the use of ensemble statistics. In practice, ensemble statistics are replaced by local spatial statistics. This method for estimating local statistics has the underlying assumption that an image is locally ergodic [33]. For example, to obtain $E[w^2]$, we can use the following maximum likelihood estimate for w Gaussian within a moving window centered in (x,y) of size $(2N+1)$ x $(2N+1)$:

$$E[w^2] = \frac{1}{(2N+1)^2} \sum_{i=-N}^{N} \sum_{j=-N}^{N} w^2(x+i, y+j) \tag{4.20}$$

For the quantity $E[uh(w)]$, $h(w)$ can be computed and is accessible but not the transformed ideal image u, therefore the following estimate is used:

$$E[uh(w)] = \frac{1}{(2N+1)^2} \sum_{i=-N}^{N} \sum_{j=-N}^{N} w(x+i, y+j) h(w(x+i, y+j)) \tag{4.21}$$

The above estimate is justified because the noise n has zero mean. Computation of $E[h^2(w)]$ is done similarly.

4.3 Multichannel Image Filtering

Since almost all practical applications now use color images, extension of the above algorithm to handle color image signals is of great importance. One obvious approach is to perform noise filtering independently in three different color channels, but this approach has a fundamental assumption that the three channels are independent and

ignore relationships among different channels. Therefore, the proposed scheme treat the signal as multivariate and has the following form:

$$\hat{\mathbf{u}} = h(\mathbf{w}) + a(\mathbf{w} - h(\mathbf{w})) \tag{4.22}$$

The above expression assumes the following noise model is valid after channel-wise generalized homomorphic transformation:

$$\mathbf{w} = \mathbf{u} + \mathbf{n} \tag{4.23}$$

with $\mathbf{w}$ being a vector of 3 (red, green, and blue) channels in the transformed optical density domain:

$$\mathbf{w} = \begin{bmatrix} w_R(x,y) \\ w_G(x,y) \\ w_B(x,y) \end{bmatrix} \tag{4.24}$$

In vector notation, the multichannel filtering scheme is:

$$\hat{\mathbf{u}} = \begin{bmatrix} \hat{u}_R \\ \hat{u}_G \\ \hat{u}_B \end{bmatrix} = \begin{bmatrix} h(w_R) \\ h(w_G) \\ h(w_B) \end{bmatrix} + a \begin{bmatrix} w_R - h(w_R) \\ w_G - h(w_G) \\ w_B - h(w_B) \end{bmatrix} \tag{4.25}$$

The discriminating function in the new filter mask is now a function of differences in three channels for a moving window $\mathbf{M}$ of size $(2N+1)$ x $(2N+1)$ centered on the current pixel (x,y):

$$h(i,j) = exp\left(-\frac{\|\mathbf{w}(i,j) - \mathbf{w}(x,y)\|^2}{b^2}\right) \tag{4.26}$$

and $\|\cdot\|$ is the Euclidean distance:

$$\begin{aligned} \|\mathbf{w}(i,j) - \mathbf{w}(x,y)\|^2 &= (w_R(i,j) - w_R(x,y))^2 + (w_G(i,j) - w_G(x,y))^2 \\ &\quad + (w_B(i,j) - w_B(x,y))^2 \end{aligned} \tag{4.27}$$

Again the filter mask $h(i,j)$ is allowed to vary from pixel to pixel, and the same weighted window is to be applied to three channels. To find the optimum expression for a, the criterion to be minimized is the following:

$$\min_{\hat{\mathbf{u}}(x,y) \in \mathbf{M}} E[\ \|\ \hat{\mathbf{u}}(x,y) - \mathbf{u}(x,y)\ \|^2\ ] \tag{4.28}$$

Thus, minimization of the above criterion yields:

$$\begin{aligned} a_{optimum} &= \frac{E[\ \|\mathbf{u}\|^2\ ] + E[\ \|h(\mathbf{w})\|^2\ ] - 2E[\ \mathbf{u}\cdot h(\mathbf{w})\ ]}{E[\ \|\mathbf{u}\|^2\ ] + E[\ \|\mathbf{n}\|^2\ ] + E[\ \|h(\mathbf{w})\|^2\ ] - 2E[\ \mathbf{u}\cdot h(\mathbf{w})\ ]} \\ &= \frac{E[\ \|\mathbf{w}\|^2\ ] - E[\ \|\mathbf{n}\|^2\ ] + E[\ \|h(\mathbf{w})\|^2\ ] - 2E[\ \mathbf{u}\cdot h(\mathbf{w})\ ]}{E[\ \|\mathbf{w}\|^2\ ] + E[\ \|h(\mathbf{w})\|^2\ ] - 2E[\ \mathbf{u}\cdot h(\mathbf{w})\ ]} \end{aligned} \tag{4.29}$$

with $\mathbf{u}\cdot h(\mathbf{w})$ denoting the dot product. To simplify the computational complexity of the parameter a, we can assume the weighted window to be the sample mean filter. The parameter will then have the following expression:

$$a_{sub\_optimum} = \frac{\sigma^2_{\mathbf{u}}(x,y)}{\sigma^2_{\mathbf{u}}(x,y) + \sigma^2_{\mathbf{n}}(x,y)} = \frac{\sigma^2_{\mathbf{w}}(x,y) - \sigma^2_{\mathbf{n}}(x,y)}{\sigma^2_{\mathbf{w}}(x,y)} \tag{4.30}$$

For the parameter b, again a good choice is the value $b^2 = \sigma^2_{\mathbf{w}}$.

The most common way to estimate the statistics of local multivariate signal (eg. $\sigma^2_{\mathbf{w}}(x,y)$) is to average over the moving window $\mathbf{M}$ [34]

$$\sigma^2_{\mathbf{w}}(x,y) = \frac{1}{(2N+1)^2} \sum_{i=-N}^{N} \sum_{j=-N}^{N} \|\ \mathbf{w}(x+i,y+j) - m_{\mathbf{w}}(x,y)\ \|^2 \tag{4.31}$$

where $m_{\mathbf{w}}(x,y)$ is the mean of the signal $\mathbf{w}$:

$$m_{\mathbf{w}}(x,y) = \frac{1}{(2N+1)^2} \sum_{i=-N}^{N} \sum_{j=-N}^{N} \mathbf{w}(x+i,y+j) \tag{4.32}$$

4.4 Film Grain Noise Generation

As outlined in Chapter 1, film grain noise generation has applications in television and motion picture productions since digitized film images, video images and computer generated images are routinely combined into one frame. In this process artificial noise is added to the video and computer generated images to match the grain pattern of

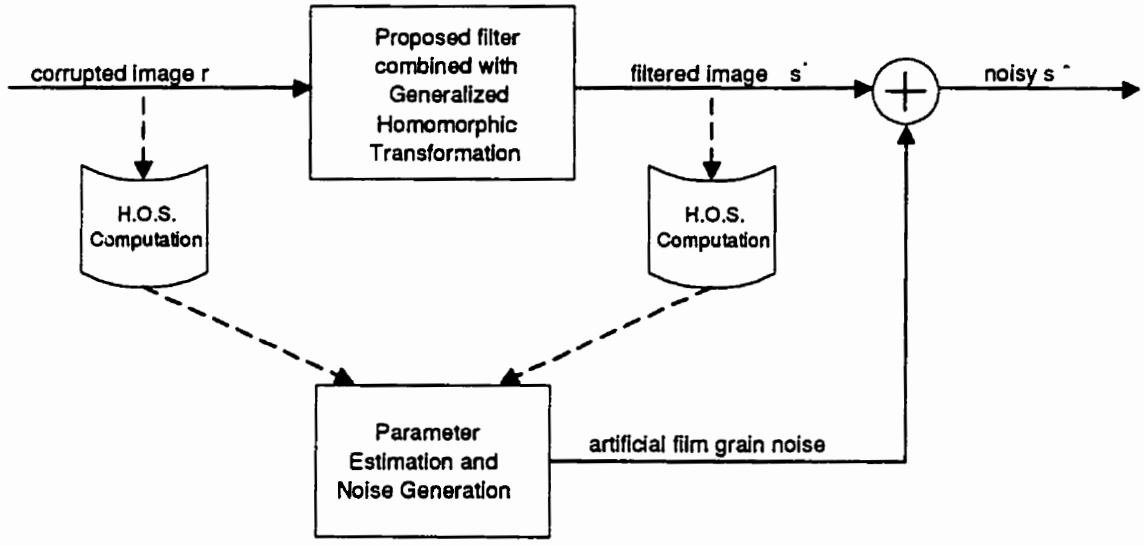

Figure 4.2: Block diagram for noise generation.

the film. To add the right amount of artificial film grain noise, the noise parameter k must be known.

One procedure to test the above noise generation method is the following. Given a noisy photographic image, perform the generalized homomorphic transformation (to decouple noise from signal), and then filter the transformed image using the proposed filter. The filtered image is transformed back and is assumed the ideal image. Then statistics of the 'ideal' and the noisy image are computed to solve for k. When k is known, add the noise back to the 'ideal' image according to Eq. (4.2) to compare the two noisy images. By modifying the weight a in the proposed filter, it is possible to perform filtering without knowing the *a prior* information regarding the noise. The weight a now has the form

$$a = \frac{\alpha}{E[w^2] + E[h^2(w)] - 2E[uh(w)]} \tag{4.33}$$

where α is the mean of the denominator of a, meaning half of the time the filter performs more smoothing and half of the time preserves edge. The noise generation procedure is shown in Fig. 4.2.

4.5 Performance Comparison

To assess performance of the new nonlinear adaptive filter, existing contrast enhancement filters like the Lee's algorithm is chosen for comparison: [30]

$$\hat{u}(x,y) = m_u(x,y) + \frac{\sigma_u^2(x,y)}{\sigma_u^2(x,y) + \sigma_n^2(x,y)}(w(x,y) - m_u(x,y)) \tag{4.34}$$

where m_w is the sample mean of the transformed image w within a moving window. The value of p for signal-dependent noise is held to be 0.5 in all cases since this is typical for a variety of film stocks [10, 11, 12, 13]. The transformation pair used is

$$g(r) = \frac{2}{k}\sqrt{r}, \tag{4.35}$$

and

$$g^{-1}(r) = (\frac{k}{2}r)^2. \tag{4.36}$$

A filter size of 3 x 3 is used throughout the simulations.

4.5.1 Grayscale Images

For gray scale images k is held to be 0.1 for moderate noise corruption. The criteria used in evaluating the performance are 1) signal-to-noise ratio (SNR), 2) mean absolute error (MAE), and 3) mean square error (MSE). All the criteria are calculated in the density domain. Four test images of size 256 x 256 were used: Lenna, Peppers, Mountain, and Melon. Results are summarized in Tables 4.1 - 4.4, and filtered Lenna images are shown in Fig. 4.4 and 4.5.

As Tables 4.1 - 4.4 show, the results obtained with the proposed algorithm are better than the Lee's algorithm in both the mean absolute error (MAE) and the mean square error (MSE). Moreover, edge preservation is satisfactory and noise smoothing using the proposed filter is better than the Lee's algorithm. This is due to the fact

that the filter mask for computing lowpass component of the proposed scheme is non-stationary for different regions. In regions near the edge less smoothing is done in the lowpass component, while in regions away from edge more smoothing is done.

To determine the sensitivity of the proposed algorithm on the *a prior* knowledge of the noise variance σ_n^2, a series of experiments were performed. Now the generalized homomorphic transformation is the square-root operation without the proportionality constant $2/k$. It was shown in Eq. (4.5) that the following is true:

$$w = \sqrt{s} + X \approx \sqrt{s} + \frac{k}{2}n = u + \frac{k}{2}n \tag{4.37}$$

Because n is zero mean and unit variance by definition, we have

$$\sigma_X^2 = E[X^2] = k^2/4 \tag{4.38}$$

and expression for a becomes:

$$a = \frac{E[w^2] - k^2/4 + E[h^2(w)] - 2E[uh(w)]}{E[w^2] + E[h^2(w)] - 2E[uh(w)]} \tag{4.39}$$

The true value of k is held to be 0.1, but the actual value used in the computation of the weight a is allowed to vary in the range 0.04-0.16 in increments of 0.02 to see the robustness of the proposed algorithm. Simulation results for two test images (Lenna and Peppers) are listed in Table 4.5.

It can be observed from Table 4.5 that the proposed scheme is more robust to the value of k used. The variation in performance for the proposed scheme is smaller. This is important, because often k (which directly affects the noise variance) is not known exactly and is estimated.

It is anticipated that in the case of severe noise conditions (which is less likely in practice), a larger filter size should be used for more noise smoothing. For completeness, the effect of filter size on performance for different noise levels was investigated. Severe noise (corresponding to a value of $k = 0.2$) is added to the image 'Lenna', and a filter size of 3 x 3 and 5 x 5 are used in the simulations. From Table 4.6, some interesting observations can be made:

- In the case of severe noise (this corresponds to $k = 0.2$) , the proposed filter does not perform as good as the existing method. To understand this, consider

filter scheme	SNR (dB)	MAE	MSE
no filtering	16.7591	4.6375e-2	3.6820e-3
Lee's	20.5460	2.7635e-2	1.5396e-3
Proposed scheme (sub-optimal solution)	20.8879	2.6434e-2	1.4230e-3
Proposed scheme (exact solution)	21.0246	2.6076e-2	1.3789e-3

Table 4.1: Performance of different filtering schemes with image 'Lenna'.

filter scheme	SNR (dB)	MAE	MSE
no filtering	15.9961	4.0384e-2	2.7924e-3
Lee's	20.3319	2.2355e-2	1.0290e-3
Proposed scheme (sub-optimal solution)	20.5840	2.1658e-2	9.7093e-4
Proposed scheme (exact solution)	20.8932	2.1008e-2	9.0420e-4

Table 4.2: Performance of different filtering schemes with image 'Peppers'.

a large value of k that corresponds to a high noise variance. Although the slope of the discriminating Gaussian function is low, meaning more averaging in the filter mask h, there exists a point where the noise is so severe that sample averaging is more effective in suppressing noise.

- A large filter size generally means more noise smoothing. For filter size 5 x 5, the proposed filter results in smaller MSE in the case of severe noise. More noise is removed, as can be seen from the SNRs of the filtered images with different filter size. It can be said that in moderate noise corruption, which is usually the case, a filter size of 3 x 3 is sufficient.

4.5.2 Computational Complexity

To obtain a rough estimate of the proposed scheme, consider a filter mask of size n x n, and an image size of M x N. The main computational load is in computing the

filter scheme	SNR (dB)	MAE	MSE
no filtering	15.9772	4.5280e-2	3.4005e-3
Lee's	21.3315	2.3135e-2	9.9110e-4
Proposed scheme (sub-optimal solution)	21.2219	2.3611e-2	1.0164e-3
Proposed scheme (exact solution)	21.7363	2.2613e-2	9.0290e-4

Table 4.3: Performance of different filtering schemes with image 'Mountain'.

filter scheme	SNR (dB)	MAE	MSE
no filtering	15.8393	3.9878e-2	2.7628e-3
Lee's	20.6913	2.1930e-2	9.0376e-4
Proposed scheme (sub-optimal solution)	21.0896	2.1008e-2	8.2456e-4
Proposed scheme (exact solution)	21.6563	1.9980e-2	7.2369e-4

Table 4.4: Performance of different filtering schemes with image 'Melon'.

Figure 4.3: Corrupted 'Lenna' with $k = 0.1$.

Figure 4.4: Filtered 'Lenna' using the Lee's algorithm.

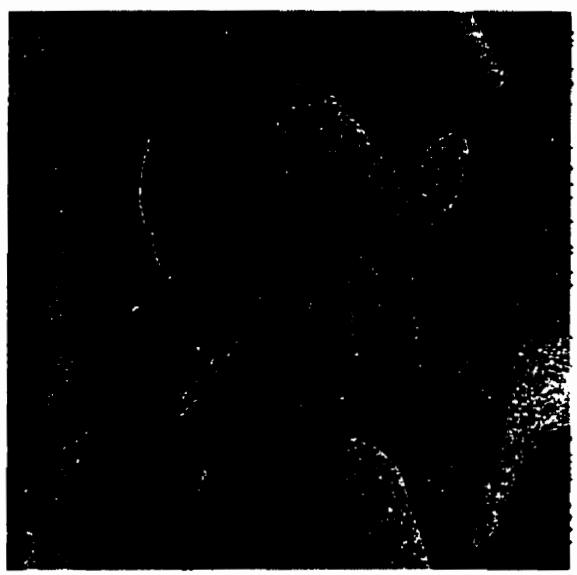

Figure 4.5: Filtered 'Lenna' using the proposed scheme (exact).

	SNR (dB) for 'Lenna'		SNR (dB) for 'Peppers'	
k	Lee's algorithm	Proposed scheme	Lee's algorithm	Proposed scheme
0.04	17.6348	18.1119	16.9616	17.4797
0.06	18.6386	19.5490	18.0904	19.0946
0.08	19.7407	20.6830	19.3628	20.4314
0.10	20.5460	21.0246	20.3319	20.8932
0.12	20.8309	21.0338	20.7663	20.9258
0.14	20.7076	21.0310	20.9259	20.9259
0.16	20.3979	21.0308	20.6449	20.9259

Table 4.5: Performance of different filtering schemes for the images 'Lenna' and 'Peppers' when the wrong k is used. The correct value of k is 0.1. SNR for the corrupted 'Lenna' is 16.76 dB, and that for the corrupted 'Peppers' is 16.00 dB.

	SNR (dB) with $k = 0.1$		SNR (dB) with $k = 0.2$	
filter size	3 x 3	5 x 5	3 x 3	5 x 5
no filtering	16.7591	16.7591	10.8349	10.8349
Lee's algorithm	20.5460	20.4159	15.7317	16.0371
Proposed scheme	21.0246	20.9123	15.0405	15.7725

Table 4.6: Effect of filter size on performance with different k.

lowpass component with filter mask h and the adaptive weight a. Two mathematical operations considered in this case are addition ($\oplus$) and multiplication ($\otimes$), with multiplication being the most costly.

In computing the lowpass component, approximately $2n^2$ additions and n^2 multiplications are needed: n^2 additions and $2n^2$ multiplications for computing the filter mask and another n^2 additions/multiplications for performing lowpass filtering. For the adaptive weight, roughly $3n^2$ additions and multiplications are required. The total number of computations per pixel for the proposed scheme is summarized in Table 4.7, with Lee's algorithm listed beside as a comparison.

Proposed filter		Lee's algorithm	
computation	no. of operations	computation	no. of operations
Lowpass	$\oplus$: $2n^2$ $\otimes$: $3n^2$	Lowpass	$\oplus$: n^2 $\otimes$: n^2
Adaptive weight	$\oplus$: $3n^2$ $\otimes$: $3n^2$	Adaptive weight	$\oplus$: n^2 $\otimes$: n^2
Total	$\oplus$: $5n^2$ $\otimes$: $6n^2$	Total	$\oplus$: $2n^2$ $\otimes$: $2n^2$

Table 4.7: Computational complexity of the proposed filter.

4.5.3 Color Images

For color images the following noise model is assumed after transformation:

$$\mathbf{w} = g(\mathbf{r}) = \mathbf{u} + \mathbf{n} \tag{4.40}$$

The transformation pair has the form:

$$g(\mathbf{r}) = \begin{bmatrix} g(r_R) \\ g(r_G) \\ g(r_B) \end{bmatrix} = \begin{bmatrix} 2\sqrt{r_R}/k_R \\ 2\sqrt{r_G}/k_G \\ 2\sqrt{r_B}/k_B \end{bmatrix} \tag{4.41}$$

and

$$g^{-1}(\mathbf{r}) = \begin{bmatrix} g^{-1}(r_R) \\ g^{-1}(r_G) \\ g^{-1}(r_B) \end{bmatrix} = \begin{bmatrix} (k_R r_R)^2/4 \\ (k_G r_G)^2/4 \\ (k_B r_B)^2/4 \end{bmatrix} \tag{4.42}$$

To select k for different channels, several issues need be considered. First, the choice of k should reflect the relative noise levels in actual color-sensitive emulsion layers that lead to amount of noise in different channels (RGB channels). Second, it should also take into account the human visual system, that is, the channel with heavy noise should have the greatest effect on perceived graininess. With the above considerations, noise power in red channel should be the least, followed by blue and green

channel [35, 36]. In simulations two sets of values of $\mathbf{k}$ are $\mathbf{k}_1$:

$$\mathbf{k}_1 = \begin{bmatrix} k_R \\ k_G \\ k_B \end{bmatrix} = \begin{bmatrix} 0.07 \\ 0.10 \\ 0.10 \end{bmatrix} \tag{4.43}$$

and $\mathbf{k}_2$:

$$\mathbf{k}_2 = \begin{bmatrix} k_R \\ k_G \\ k_B \end{bmatrix} = \begin{bmatrix} 0.10 \\ 0.15 \\ 0.15 \end{bmatrix} \tag{4.44}$$

Different algorithms were selected for noise filtering:

- 3 independent runs of Lee's algorithm for single-channel filtering
- 1 run of Lee's algorithm for multichannel filtering
- 3 independent runs of proposed algorithm for single-channel filtering
- 1 run of proposed algorithm for multichannel filtering

Simple extension of the Lee's algorithm for grayscale images to color image gives:

$$\hat{\mathbf{u}}(x,y) = m_{\mathbf{u}}(x,y) + \frac{\sigma^2_{\mathbf{u}}(x,y)}{\sigma^2_{\mathbf{u}}(x,y) + \sigma^2_{\mathbf{n}}(x,y)}(\mathbf{w}(x,y) - m_{\mathbf{u}}(x,y)) \tag{4.45}$$

Two test color images are used: 'Lenna' and 'Melon' (see Fig. 4.6 - 4.7). Two popular metrics used in evaluating the distance (and hence the performance) between the ideal image and the filtered image are 1) the L_1 norm and 2) the L_2 norm, defined as: [37]

$$L_1 \text{ norm} = |s_R - \hat{s_R}| + |s_G - \hat{s_G}| + |s_B - \hat{s_B}| \tag{4.46}$$

and

$$L_2 \text{ norm} = \sqrt{(s_R - \hat{s_R})^2 + (s_G - \hat{s_G})^2 + (s_B - \hat{s_B})^2} \tag{4.47}$$

All the criteria are calculated in the density domain. Results are summarized in Tables 4.8 and 4.9 for filter size of 3 x 3. Corrupted and filtered images are depicted in

Fig. 4.8 - 4.10.

It can be observed that for both moderate and large noise power ($\mathbf{k}_1$ and $\mathbf{k}_2$), the proposed multichannel scheme has excellent noise suppression over single channel filtering scheme. This is because information between channels is utilized in computing the filter mask and the adaptive weight. Moreover, the proposed multichannel scheme outperforms the Lee's algorithm in both noise smoothing and edge preservation.

4.5.4 Film Grain Noise Generation

To test the noise generation procedure, the image 'Lenna' is used for noise generation in grayscale and in color. Film grain noise with $k = 0.1$ is added to the ideal image and the corrupted image is filtered using the modified proposed algorithm. Then k is computed using fourth-order statistics of the two images. Although k can be solved by matching their variances, it was found that variance of the filtered image is lower than that of the corrupted image because edges are blurred to some extent. Thus using variance to obtain k would lead to over-estimation, and the final image would be too noisy. To compare the noise level of the original corrupted and the final image, single-channel and multichannel mean square error (MSE) were used. Multichannel MSE is defined as the sum of the three signal-channel MSE's. For the original corrupted image the signal power is the ideal signal power, whereas the signal power of the final image is that of the filtered image. In the case of color images, the corrupted image with $\mathbf{k}_1 = [0.07 \quad 0.1 \quad 0.1]^T$ is filtered independently in each channel. Both grayscale images are shown in Fig. 4.11. MSE's of noise-added grayscale and color images are listed in Tables 4.10. It can be observed that not only both the original and noise-added images are similar in appearance, but also they have similar noise level as well.

	$\mathbf{k}_1$		$\mathbf{k}_2$	
Metric	L_1 *norm*	L_2 *norm*	L_1 *norm*	L_2 *norm*
no filtering	1.1962e-1	9.4434e-2	1.7836e-1	1.4154e-1
Lee's (single-channel)	7.2873e-2	6.1423e-2	9.8572e-2	8.3698e-2
Lee's (multichannel)	7.1060e-2	6.0018e-2	9.5113e-2	8.0531e-2
Proposed scheme (single-channel)	7.0978e-2	5.9972e-2	1.0284e-1	8.6439e-2
Proposed scheme (multichannel)	6.6231e-2	5.6045e-2	8.8142e-2	7.3373e-2

Table 4.8: Performance of different filtering schemes with color 'Lenna'.

	$\mathbf{k}_1$		$\mathbf{k}_2$	
Metric	L_1 *norm*	L_2 *norm*	L_1 *norm*	L_2 *norm*
no filtering	1.1903e-1	9.4497e-2	1.7731e-1	1.4092e-1
Lee's (single-channel)	7.0296e-2	5.8016e-2	9.3516e-2	7.7756e-2
Lee's (multichannel)	6.8166e-2	5.6054e-2	8.9841e-2	7.4023e-2
Proposed scheme (single-channel)	6.4591e-2	5.2762e-2	9.4298e-2	7.7939e-2
Proposed scheme (multichannel)	6.1034e-2	4.9899e-2	8.1438e-2	6.5996e-2

Table 4.9: Performance of different filtering schemes with color 'Melon'.

statistics	Single channel MSE	Multichannel MSE
second order	4.2929e-3	1.1550e-2
third order	4.5206e-3	1.1570e-2
fourth order	3.5062e-3	9.7017e-3

Table 4.10: MSE's of noise-added Lenna images. Single channel MSE for the original corrupted image is 3.68e-3, while multichannel MSE for the original corrupted color image is 8.92e-3.

Figure 4.6: Test image: color 'Lenna'.

Figure 4.7: Test image: color 'Melon'.

Figure 4.8: Corrupted color 'Lenna' with noise parameters $\mathbf{k}_2 = [0.10\ 0.15\ 0.15]^T$.

Figure 4.9: Image filtered using the Lee's algorithm (multichannel).

Figure 4.10: Image filtered using the proposed filter (multichannel).

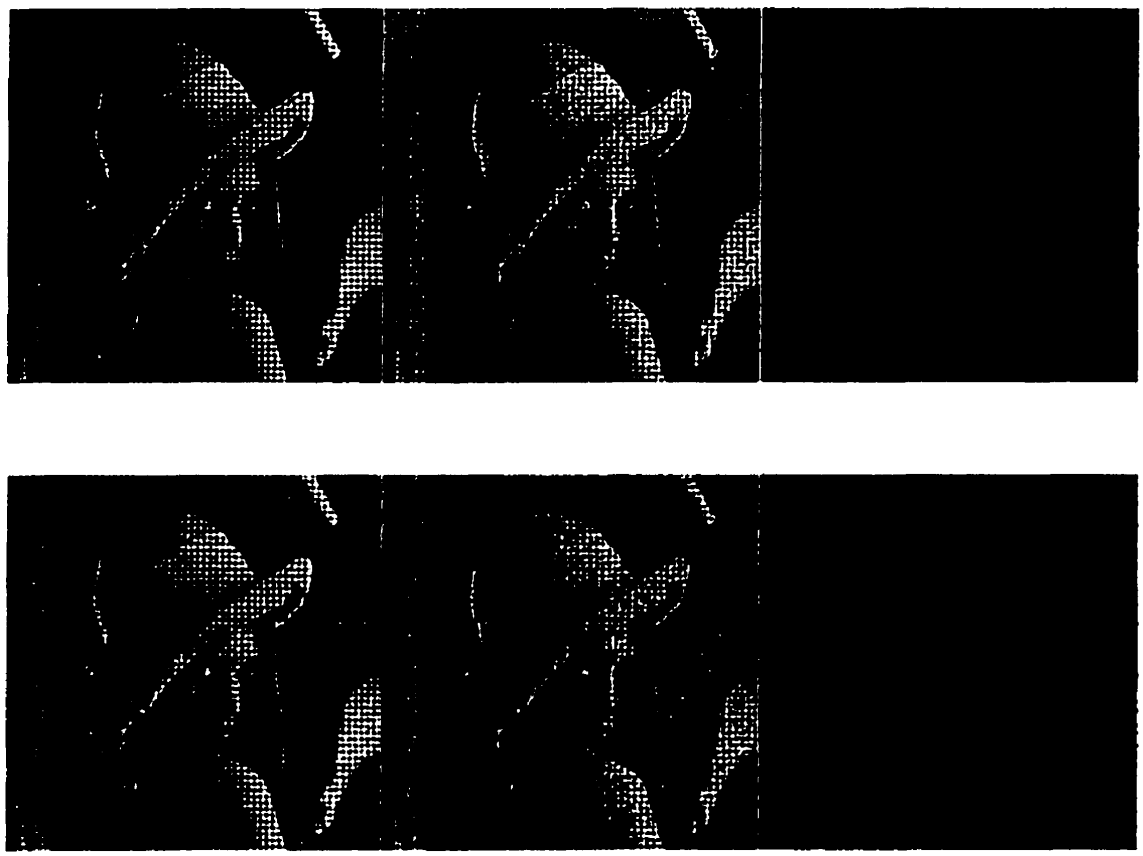

Figure 4.11: Comparsion of images generated by the proposed noise generation technique. The upper three images are the ideal (above left), corrupted (above middle), and noise image of 'Lenna' (above right). Filtered image (below left), noise added to filtered 'Lenna' (below middle) and noise image (below right) are shown below.

Chapter 5

Conclusions

5.1 Summary and Conclusions

The aims of the research were to examine statistical properties of film grain noise, and to investigate new algorithms for noise filtering and generation.

These objectives were accomplished by employing higher-order statistics (H.O.S.) of the non-Gaussian image and signal-dependent film grain noise. By using the property that any Gaussian process has zero skewness and kurtosis, statistical nature of actual film grain noise in photographic images was investigated. A more general noise distribution, namely the generalized Gaussian distribution (GGD), was assumed, and parameters of this noise distribution were estimated. It was found that under high signal densities, film grain noise exhibited non-Gaussian behavior. Nonetheless, over a practical range of signal Gaussian behavior was observed.

For noise filtering, two new methods have been proposed. The first method is based on extending the use of second-order statistics to H.O.S. A higher-order statistics based criterion was optimized and a cumulant-based Wiener-Hopf equation was used to solve for the optimum filter coefficients. It was found that this new filter has performance comparable to the familiar Wiener filter. On average the new filter

outperformed the Wiener filter by approximately 1 dB in SNR. Because of the computational load of the H.O.S. based filter, a different approach was proposed. The first step in noise filtering is to first perform a generalized homomorphic transformation to decouple the noise from the signal, and then filter the transformed image using a new local-statistics based technique. The filter mask is non-stationary and adaptive to signal activities for a balance of edge preservation and noise suppression. This approach can be extended to multivariate signals (i.e. color images) and showed some promising results. An almost 1 dB SNR improvement by this new filter over existing one was observed in the case of grayscale images. For color images, as much as 12% less error (in terms of L_2 norm) was achieved by this filter over existing one. Moreover, the proposed filter has been shown to have excellent edge preservation and noise smoothing properties.

Comparsion of these two proposed filters shows that while the H.O.S. based filter uses the 'global' image statistics, the other utilizes the local-statistics of the image. Because the adaptive filter used local-statistics, a good balance between edge preservation and noise suppression in moderate noise corruption was acheived. In terms of computational complexity, the H.O.S. based filter requires more computations than the adaptive local-statistics based filter in estimating signal statistics and computing filter coefficients. However, the H.O.S. based filter was shown to be more insensitive to the noise level. In the case of severe noise corruption (low SNR), the H.O.S. based filter still performed satisfactorily, but the local-statistics based filter did not perform well.

For film grain noise generation, a new procedure has been proposed and successfully applied in grayscale and color images. To test the validity of this procedure, photographic images were filtered using the proposed local-statistics filter and then the filtered image was assumed the 'ideal image'. A method to estimate the noise parameter using H.O.S. was proposed so that artificial noise can be added to the 'ideal image'. It was found that these two images (corrupted photographic image and filtered image with artificial noise added) have similar visual appearance and noise level.

5.2 Further Research

Below is a list of possible improvements that require further research:

1. For more accurate extraction of actual film grain noise, film negative should be scanned and digitized instead of the print. With our available equipment, scanning the photographic print is the only option.

2. Extension of the H.O.S. based filter to multichannel signals. Current research has been limited to single channel, two-dimensional signals only. Because color images can be modeled as tri-channel two-dimensional signals, definitions of the proposed filter can be extended to the case of multichannel images by exploiting the algebraic properties of Kronecker products.

3. A better way to completely decouple signal-dependent noise from signal is desired. The generalized homomorphic transformation can only approximately separate noise from signal by using a memoryless transformation to stablize its variance. Nonlinear transformation with memory may provide a better solution.

4. Procedure for noise generation can be refined. In particular, noise generation can be done by matching cumulants of actual film grain noise to the cumulants of the output of a multichannel linear system driven by a stochastic input. Current noise generation technique is limited to matching the magnitude of the noise. By incorporating spectral and magnitude dependence of noise on image, a more realistic result is anticipated.

5. The proposed noise filtering and generation algorithms can be applied equally to other signal-dependent noises like speckle [38] (modeled as multiplicative with gamma distribution), photoelectronic shot noise [10] (modeled as Poisson photocounting process), and magnetic tape noise [14]. For example, the generalized homomorphic transformation combined with the proposed local-statistics filter can be used to handle different types of signal-dependent noise.

Appendix A

Detailed Derivations

A.1 Proof of Eq. (3.10)

To show the filter satisfying the cumulant based orthogonality condition is optimum, e_{xy} is first expressed as:

$$\begin{aligned} e_{xy} &= s_{xy} - \sum_{i=a}^{b}\sum_{j=c}^{d} h_{ij} r_{x-i,y-j} \\ &= s_{xy} - \sum_{i=a}^{b}\sum_{j=c}^{d} \tilde{h}_{ij} r_{x-i,y-j} + \sum_{i=a}^{b}\sum_{j=c}^{d} (\tilde{h}_{ij} - h_{ij}) r_{x-i,y-j} \\ &= \tilde{e}_{xy} + \sum_{i=a}^{b}\sum_{j=c}^{d} (\tilde{h}_{ij} - h_{ij}) r_{x-i,y-j} \end{aligned} \tag{A.1}$$

Then

$$\begin{aligned} J_C^M &= \left\{ \sum_{\alpha}\sum_{\beta} Cum^M(e_{xy}, e_{xy}, r_{x-\alpha,y-\beta}, \ldots, r_{x-\alpha,y-\beta}) \right\}^2 \\ &= \left\{ \sum_{\alpha}\sum_{\beta} Cum^M(\tilde{e}_{xy}, \tilde{e}_{xy}, r_{x-\alpha,y-\beta}, \ldots, r_{x-\alpha,y-\beta}) \right. \\ &\quad \left. + \sum_{i}\sum_{j} (\tilde{h}_{ij} - h_{ij}) \sum_{\alpha}\sum_{\beta} Cum^M(r_{x-i,y-j}, \tilde{e}_{xy}, r_{x-\alpha,y-\beta}, \ldots, r_{x-\alpha,y-\beta}) \right. \end{aligned}$$

$$
\begin{aligned}
&+\sum_i\sum_j(\tilde{h}_{ij}-h_{ij})\sum_\alpha\sum_\beta Cum^M(\tilde{e}_{xy},r_{x-i,y-j},r_{x-\alpha,y-\beta},\ldots,r_{x-\alpha,y-\beta})\\
&+\sum_i\sum_j\sum_k\sum_l(\tilde{h}_{ij}-h_{ij})(\tilde{h}_{kl}-h_{kl})*\\
&\sum_\alpha\sum_\beta Cum^M(r_{x-i,y-j},r_{x-k,y-l},r_{x-\alpha,y-\beta},\ldots,r_{x-\alpha,y-\beta})\Big\}^2\\
=\;&\Big\{\sum_\alpha\sum_\beta Cum^M(\tilde{e}_{xy},\tilde{e}_{xy},r_{x-\alpha,y-\beta},\ldots,r_{x-\alpha,y-\beta})\Big\}^2 \text{ since (Eq. 3.9)}\\
=\;&\Big\{\sum_\alpha\sum_\beta Cum^M(\tilde{e}_{xy},s_{xy}-\sum_i\sum_j\tilde{h}_{ij}r_{x-i,y-j},r_{x-\alpha,y-\beta},\ldots,r_{x-\alpha,y-\beta})\Big\}^2\\
=\;&\Big\{\sum_\alpha\sum_\beta Cum^M(\tilde{e}_{xy},s_{xy},r_{x-\alpha,y-\beta},\ldots,r_{x-\alpha,y-\beta})\\
&-\sum_i\sum_j\tilde{h}_{ij}\sum_\alpha\sum_\beta Cum^M(\tilde{e}_{xy},r_{x-i,y-j},r_{x-\alpha,y-\beta},\ldots,r_{x-\alpha,y-\beta})\Big\}^2\\
=\;&\Big\{\sum_\alpha\sum_\beta Cum^M(\tilde{e}_{xy},s_{xy},r_{x-\alpha,y-\beta},\ldots,r_{x-\alpha,y-\beta})\Big\}^2 \text{ since (Eq. 3.9)} \qquad \text{(A.2)}
\end{aligned}
$$

Thus for $h_{ij}=\tilde{h}_{ij}$,

$$
J^M_{Cmin}=\Big\{\sum_\alpha\sum_\beta Cum^M(\tilde{e}_{xy},s_{xy},r_{x-\alpha,y-\beta},\ldots,r_{x-\alpha,y-\beta})\Big\}^2 \qquad \text{(A.3)}
$$

A.2 Derivation of Eq. (4.15) and Eq. (4.29)

The following is the detailed derivation for Eq. (4.15) and Eq. (4.29). First we begin with the case of single-channel image. Expand the expression for mean square error (MSE):

$$
\begin{aligned}
MSE &= E[(u-\hat{u})^2]\\
&= E[u^2-2u\hat{u}+\hat{u}^2]\\
&= E[u^2-2u(h(w)+a(w-h(w))+h^2(w)+2awh(w)-2ah^2(w)\\
&\quad +a^2(w^2-2wh(w)+h^2(w))]\\
&= E[u^2]-2E[uh(w)]+E[h^2(w)]
\end{aligned}
$$

$$+ 2a(E[uh(w)] - E[uw] + E[wh(w)] - E[h^2(w)])$$
$$+ a^2(E[w^2] - 2E[wh(w)] + E[h^2(w)]) \tag{A.4}$$

Taking the derivative of MSE and set it to zero yields:

$$\begin{aligned}\frac{\partial MSE}{\partial a} &= 2(2E[uh(w)] - E[uw] - E[h^2(w)] \\ &\quad + 2a(E[w^2] - 2E[uh(w)] + E[h^2(w)]) \\ &= 0\end{aligned} \tag{A.5}$$

Therefore a becomes:

$$\begin{aligned}a &= \frac{E[u^2] + E[h^2(w)] - 2E[uh(w)]}{E[w^2] + E[h^2(w)] - 2E[uh(w)]} \\ &= \frac{E[w^2] - E[n^2] + E[h^2(w)] - 2E[uh(w)]}{E[w^2] + E[h^2(w)] - 2E[uh(w)]}\end{aligned} \tag{A.6}$$

as in Eq. (4.15).

For multichannel image, expression for a is obtained similarly. Observe that

$$E[\ \| \hat{\mathbf{u}} - \mathbf{u} \|^2\ ] = E[(u_R - \hat{u}_R)^2] + E[(u_G - \hat{u}_G)^2] + E[(u_B - \hat{u}_B)^2] \tag{A.7}$$

then expanding the above leads to an expression similar to Eq. (A.4). Following the same approach and using vector notation, Eq. (4.29) results.

Bibliography

[1] R. Kasturi and J. F. Walkup, "Nonlinear Image Restoration in Signal-Dependent Noise", *Advances in Computer Vision and Image Processing*, Vol. 2, pp. 213-273, (1986).

[2] R. C. Gonzalez and R. E. Woods, *Digital Image Processing*, Addison Wesley, pp.71-75, (1992).

[3] H. C. Andrews and B. R. Hunt, *Digital Image Restoration*, Prentice-Hall, Inc., p.17-24 (1977).

[4] C. E. K. Mees, *The Theory of the Photographic Process*, 4th edition, Macmillan Publishing Co., Inc., pp.618-624, (1977).

[5] A. E. Saunders, "Mathematical Quirks of Photographic Science", *J. Photogr. Sci.* Vol. 42, pp. 142-148, (1994).

[6] E. A. Trabka, "Crowded Emulsions: Granularity Theory for Monolayers", *J. Opt. Soc. Am.*, Vol. 61, pp. 800-810, (1971).

[7] E. A. Trabka, "Crowded Emulsions: Granularity Theory for Multilayers", *J. Opt. Soc. Am.*, Vol. 62, pp. 659-667, (1972).

[8] S. A. Benton, "Properties of Granularity Wiener Spectra", *J. Opt. Soc. Am.*, Vol. 61, pp. 524-529, (1971).

[9] T. Hattori, R. Ohsato, and M. Inui, "The Simulation of Granular Noise in Colour Negative Film: Integrating Magnitude and Spectral Component Dependence", *Konica Technical Report*, Vol. 6, Janurary, (1993).

[10] J. F. Walkup and R. C. Choens, "Image Processing in Signal-Dependent Noise", *Opt. Eng.* Vol. 13, pp. 258-266, (1974).

[11] J. D. Downie and J. F. Walkup, "Optimal Correlation Filters for Images with Signal-Dependent Noise", *J. Opt. Soc. Am. A*, Vol. 11, pp. 1599-1609, (1994).

[12] H. H. Arsenault and M. Levesque, "Combined Homomorphic and Local-Statistics Processing for Restoration of Images Degraded by Signal-Dependent Noise", *Appl. Opt.* Vol. 23, pp. 845-850, (1984).

[13] H. H. Arsenault and M. Denis, "Image Processing in Signal-Dependent Noise", *Can. J. Phy.*, Vol. 61, pp. 309-317, (1983).

[14] G. K. Froehlich, J. F. Walkup, and R. B. Asher, "Optimal Estimation in Signal-Dependent Noise", *J. Opt. Soc. Am.*, Vol. 68, pp. 1665-1672, (1979).

[15] F. Naderi and A. A. Sawchuk, "Estimation of Images Degraded by Film-Grain Noise", *Appl. Opt.*, Vol. 17, pp. 1228-1237, (1978).

[16] D. G. Falconer, "Image Enhancement and Film-Grain Noise", *Optica Acta*, Vol. 17, pp. 693-705, (1970).

[17] G. K. Froehlich, J. F. Walkup, and T. F. Krile, "Estimation in Signal- Dependent Film-Grain Noise", *Appl. Opt.*, Vol. 20, pp. 3619-3626, (1981).

[18] H. H. Arsenault and G. April, "Properties of Speckle Integrated with a Finite Aperture and Logarithmically Transformed", *J. Opt. Soc. Am.*, Vol. 66, pp. 1160-1163, (1976).

[19] H. H. Arsenault, C. Gendron, and M. Denis, "Transformation of Film-Grain Noise into Signal-Independent Additive Gaussian Noise", *J. Opt. Soc. Am.*, Vol. 71, pp. 91-94, (1981).

[20] H. H. Arsenault and M. Denis, "Integral Expression for Transformating S-gnal-Dependent Noise into Signal-Independent Noise", *Opt. Lett.*, Vol. 6, pp. 210-212, (1981).

[21] M. Denis and H. H. Arsenault, "On the Accuuracy of A Method to Make Film-Grain Noise Independent of the Signal", *Opt. Comm.*, Vol. 38, pp. 166-169, (1981).

[22] D. Hatzinakos, "Higher-Order Spectral (H.O.S.) Analysis", *Control and Dynamic Systems*, Vol. 65, pp. 115-168, (1994).

[23] J. M. Mendel, "Tutorial on Higher-Order Statistics (Spectra) in Signal Processing and System Theory: Theoretical Results and Some Applications", *Proc. IEEE*, Vol. 79, pp. 278-305, (1991).

[24] M. K. Varanasi and B. Aazhang, "Parametric Generalized Gaussian Density Estimation", *J. Acoust. Soc. Am.*, Vol. 86(4), pp. 1403-1415, October (1989).

[25] W. H. Pun and B. D. Jeffs, "Adaptive Image Restoration Using a Generalized Gaussian Model for Unknown Noise", *IEEE Trans. Image Processing*, Vol. 4, pp.1451-1456, (1995).

[26] C. L. Nikias and A. P. Petropulu, *Higher-Order Spectral Analysis: A Nonlinear Signal Processing framework*, Prentice Hall, Englewood Cliffs, New Jersey, (1993).

[27] C. Y. Chi and W. J. Chang, "New Higher-Order Statistics Based Criteria for the Design of Linear Prediction Error Filters", *Proc. IEEE Signal Processing Workshop on Higher-Order Statistics*, South Lake Tahoe, California, June 7-9, pp. 106-110, (1993).

[28] C. C. Feng and C. Y. Chi, "Design of Wiener Filters Using a Cumulant Based MSE Criterion", *Signal Processing*, Elseview, Vol. 54, pp.23-48, (1996).

[29] R. Ding and A. N. Venetsanopoulos, "Generalized Homomorphic and Adaptive Order Statistic Filter for the Removal of Impulsive and Signal-Dependent Noise", *IEEE Trans. Circuits and Systems*, Vol. CAS-34, No. 8, pp. 948-955, (1987).

[30] J. S. Lee, "Digital Image Enhancement and Noise Filtering by Use of Local Statistics", *IEEE Trans. Pattern Anal. Mach. Intell.*, Vol. PAMI-2, pp. 165-168, (1980).

[31] A. Kh. Al Jabri, S. A. Alshebeili, and A. N. Venetsanopoulos, "Efficient Algorithms for Computing Third and Fourth Order Cumulants", submitted to *Signal Processing*, Elsevier, under review.

[32] S. Guillon, P. Baylou, and M. Najim, "Robust Nonlinear Contrast Enhancement Filters", *Proc. of ICIP 1996*, (1996).

[33] D. T. Kuan, A. A. Sawchuk, and T. C. Strand, "Adaptive Noise Smoothing Filter for Images with Signal-Dependent Noise", *IEEE Trans. Pattern Anal. Mach. Intell.*, Vol. PAMI-7, pp. 165-177, (1985).

[34] K. Tang, J. Astola, and Y. Neuvo, "Adaptive Nonlinear Multivariate Image Filtering for Mixed Noise Removal", *Proc. of ICASSP 1993*, pp. 427-430, (1993).

[35] G. G. Attridge and M. R. Pointer, "Colour Science in Photography", *J. Photogr. Sci.*, Vol. 42, pp.197-209, (1994).

[36] M. P. Tyrrell, R. E. Jacobson, M. R. Pointer, and G. G. Attridge, "A Study of Color-Film Granularity and Print-Image Graininess", *J. Photogr. Sci.*, Vol. 41, pp. 48-55, (1993).

[37] O. D. Faugeras, "Digital Color Image Processing Within the Framework of a Human Visual Model", *IEEE Trans. ASSP*, Vol. ASSP-27, No. 4, pp. 380-393, (1979).

[38] H. H. Arsenault and G. April, "Properties of Speckle Integrated with a Finite Aperture and Logarithmically Transformed", *J. Opt. Soc. Am.*, Vol. 66, pp. 1160-1163, (1976).

[39] I. Pitas and A. N. Venetsanopoulos, *Nonlinear Digital Filters - Principles and Applications*, Kluwer Academic Publishers, 1990.

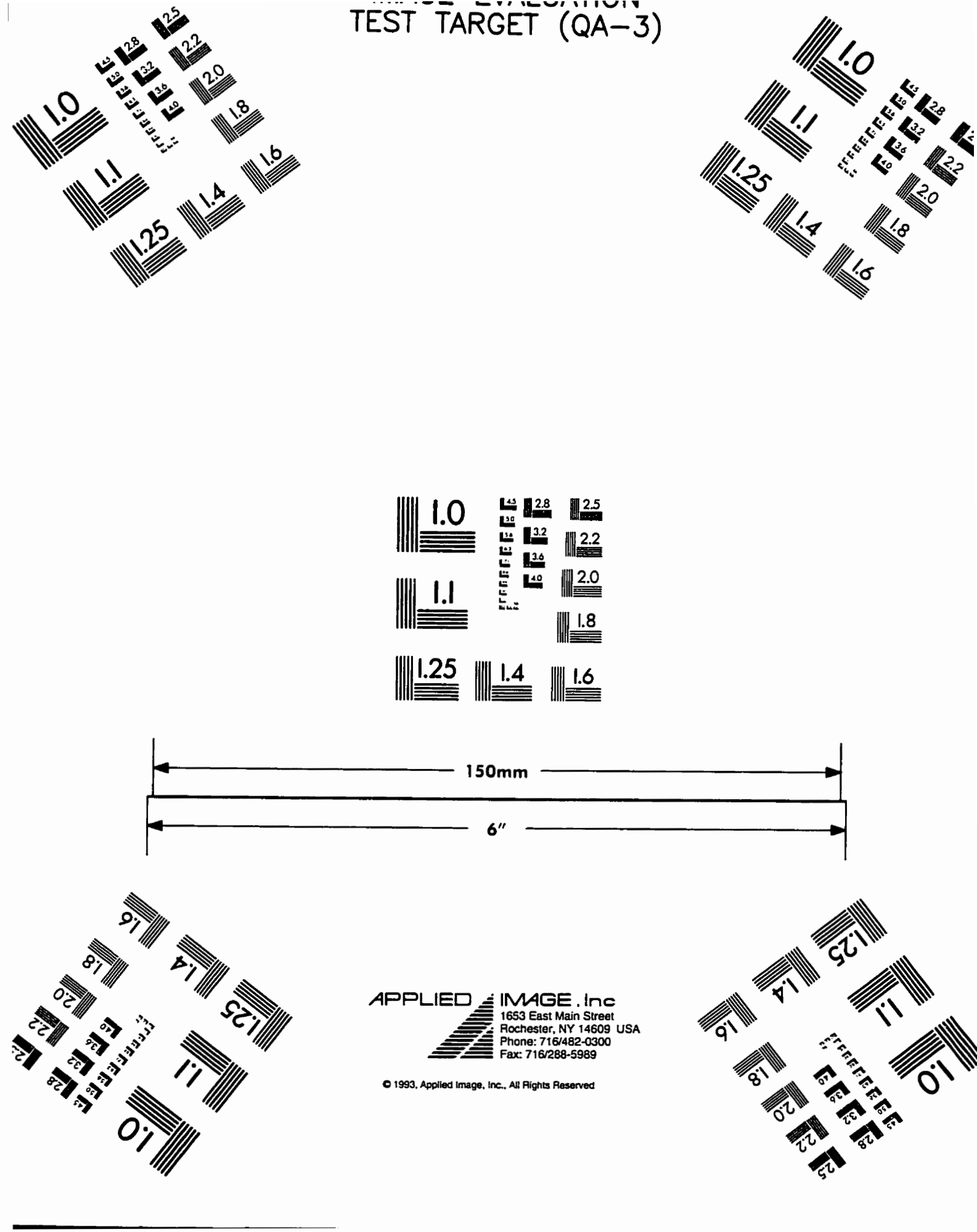
TEST TARGET (QA-3)
1.0
1.1
1.25
1.4
1.6
1.8
2.0
2.2
2.5
2.8
3.2
3.6
4.0
150mm
6"
APPLIED IMAGE, Inc
1653 East Main Street
Rochester, NY 14609 USA
Phone: 716/482-0300
Fax: 716/288-5989
© 1993, Applied Image, Inc., All Rights Reserved